MDPI

Article

Green Synthesis of Surface Modified Biochar for Simultaneous Removal of Steroidal Hormones and Heavy Metals from Wastewater: Optimisation by Central Composite Design

Sefiu Olaitan Amusat [1] , Temesgen Girma Kebede [1,*], Edward Ndumiso Nxumalo [2], Simiso Dube [1] and Mathew Muzi Nindi [2,*]

1 Department of Chemistry, College of Science, Engineering, and Technology, The Science Campus, University of South Africa, Florida 1709, South Africa; 63584484@mylife.unisa.ac.za (S.O.A.); dubes@unisa.ac.za (S.D.)

2 Institute for Nanotechnology and Water Sustainability (iNanoWS), College of Science, Engineering, and Technology, The Science Campus, University of South Africa, Florida 1709, South Africa; nxumaen@unisa.ac.za

* Correspondence: 49055313@mylife.unisa.ac.za (T.G.K.); nindimm@unisa.ac.za (M.M.N.)

Abstract: The modification of pristine biochar derived from the waste of sweet prickly pear using the green modification method to produce nano-sized biochar (nanobiochar) for the removal of steroidal hormones and heavy metals from water and wastewater is reported in this study. Based on the characterisation results using FTIR, Raman spectroscopy, and XPS, the material had (COOH), (C=O), and (OH) functional groups typical of graphitic amorphous carbon. The SEM-EDS and XRD results showed that the material was mesoporous and amorphous in nature. The BET analysis results revealed that the surface area significantly increased from 220.1 m^2/g to 354.6 m^2/g after the modification of the pristine biochar. Based on the TGA-DSC results, the material was thermally stable up to 550 °C. A complete factorial experimental design using Minitab 21 Statistical Software (version 18.1) was employed to optimise the experimental adsorption conditions. The F-values and *p*-values for the lack-of-fit of the model showed the acceptability and significance of the ANOVA model. The Freundlich adsorption isotherm was found to provide a better fit for the steroid adsorption data than the Langmuir adsorption isotherm, with moderate values of $R^2 \geq 0.92$ for Langmuir and $R^2 \geq 0.95$ for Freundlich, as well as maximum adsorption capacities of 14.53 mg/g, 10.58 mg/g, 12.50 mg/g, 5.73 mg/g, 5.63 mg/g, and 9.75 mg/g obtained for estriol, α-oestradiol, β-oestradiol, testosterone, progesterone, and bisphenol A. Freundlich R^2 values were lower than Langmuir R^2 values for metal adsorption, with maximum adsorption capacities of 8.58 mg/g, 4.15 mg/g, and 6.95 mg/g obtained for nickel, cadmium, and lead, respectively. The maximum percentage of removal for effluents and influents was between 84–89% and 78–86% for steroid hormones and heavy metals, respectively. The highest removal percentage between 90–95% was obtained for spiked ultrapure water for both steroid hormones and heavy metals. The material exhibited a removal percentage up to 60% after the first four cycles.

Keywords: ball-milled biochar; steroid hormones; adsorption; surface response; water treatment; heavy metals

1. Introduction

Access to a clean and affordable water supply (SDG Goal 6) is one of the sustainable development goals (SDGs) adopted by the United Nations in 2015, with Target 6.1: By 2030, achieve universal and equitable access to safe and affordable drinking water for all. Increased urbanisation has an impact on water quality because pollutants generated in cities settle and pollute water and because cities, industries, and agriculture are competing for more water [1]. Health issues are becoming more prevalent due to worldwide population

growth, pollution, and inadequate sanitation practices [2]. Steroid hormones have emerged as a class of potential environmental pollutants of concern in recent decades owing to their detection in the aquatic environment and their potential adverse physiological effects on species and water bodies [3]. In aquatic life, animals, and perhaps humans, steroid hormones, both naturally derived and synthetic, have great potential to interrupt normal hormonal functions such as development, metabolism, and other bodily functions or processes, especially during crucial developmental periods [4]. Steroid hormones are not eliminated during conventional wastewater treatment, according to literature reports, and are eventually discharged into the aquatic environment [5]. Exposure to wastewater effluents containing steroid hormone concentrations as low as 0.1–4.2 ng/L can disrupt the normal functionality of the endocrine systems of fish and wildlife, thereby disrupting reproduction and development [6]. Male feminisation and vitellogenin production occur as a result, reducing the rate of egg fertilisation [7].

Only a few researchers have delved into the human health risks of being exposed to natural and synthetic steroid hormones in the environment. There could be a connection between the 17-α oestradiol (E2) metabolite 16-hydroxy-E2 and breast cancer, as well as an elevated risk of liver adenomas and hepatocellular carcinomas linked with long-term usage of 17-α ethinyloestradiol (EE2) [8]. Increased amounts of androgens may contribute to the pathogenesis of prostate cancer, according to epidemiological observations [9]. Moreover, investigations have revealed that prepubescent children who are exposed to low levels of testosterone exhibit early puberty [10]. Other studies have concluded that environmental sources of steroid hormones pose little harm to people when compared to typical body oestrogen concentrations, based on worst-case exposure estimations [11]. Several researchers have reported the occurrence of steroid hormones among the emerging contaminants found in wastewater treatment plants (WWTPs) [12,13]. More recently, Mhuka et al. reported the occurrence of pharmaceuticals and personal care products in the wastewater and receiving waters in South Africa [14]. According to the report, oestradiol, which is one of the steroid hormones, was found as one of the major contaminants with the highest concentrations (2.45 µg/L) in the effluent sample from a South African WWTP. Therefore, it is vital to find effective ways for removing steroid hormones from wastewater before WWTP effluents are released into the environment.

Similarly, water supply sources worldwide are contaminated with heavy metals [15]. The presence of heavy metals in the environment is pervasive; they may be released by mining and pesticide usage, or they may just exist naturally [16]. Human exposure to harmful heavy metals has increased because of an increase in energy production due to global demand and exponential growth in the usage of heavy metals in industrial processes [17]. Prominent metals such as lead (Pb^{2+}), cadmium (Cd^{2+}), and other heavy metals that pollute aquatic systems have drawn a lot of attention from our society due to their persistence in the environment and harmful impacts on health, causing birth abnormalities and damage to numerous organs [18]. For example, lead has significant toxic effects on the immune system, neurological system, reproductive system, and kidneys [16]. Cationic heavy metals and arsenic frequently coexist in contaminated water [19].

Physical techniques, biodegradation, and chemical technologies are prominent among the traditional and modern techniques for removing heavy metals and steroid hormones from contaminated wastewater [20].

Some methods, including electrochemical treatment [21], chemical precipitation [22], solvent extraction [23], ion exchange [24], membrane filtration [25,26], reverse osmosis [27], and adsorption [28], have been used. Adsorption is regarded as an interesting and efficient approach among these technologies because of its flexibility, simplicity of operation, and relatively low cost. Due to its highly apparent advantages, such as ease of access, simplicity, environmentally friendly nature, and removal efficiency, the adsorption method has attracted a lot of attention. Based on the existing literature, numerous adsorbents have been utilised for the removal of steroid hormones from polluted wastewater [29]. In the past, adsorption methods have been used to remove steroid hormones from aqueous solutions

using activated carbon (AC), chitin, carbon nanotubes, chitosan, resin, graphene nanomaterial ion exchange, and single-walled or multi-walled carbon nanotubes [30]. However, the operational implementation of these adsorbents will be limited due to resource limitations, cumbersome production processes, and/or limited adsorption capacity of these adsorbents. Consequently, low-cost and simple-to-fabricate materials are being used to remove steroid hormones from aqueous solutions [31].

In the decontamination of heavy metals, a variety of common functional materials, such as natural mineral materials and synthetic nanomaterials, have been extensively employed. However, the key difficulty remains designing a cost-effective and long-lasting adsorbent. By harnessing the large specific surface area, high porosity, and physicochemical stability of biochar, researchers are exploring its potential as an alternative, low-cost adsorbent for removing steroids from aqueous systems. However, as common adsorbents are widely used, high costs are associated with their production, and raw materials are relatively expensive. It is important to note that the efficiency of adsorptive materials can vary depending on the specific pollutants, their concentrations, and the wastewater characteristics. Numerous adsorptive materials have been developed for the elimination of organic pollutants like dye and phenol from wastewater, such as nanocomposite, resin, and neem leaves [32–34].

Biochar has distinctive advantages such as abundant feedstock and low cost and is likely the most suitable adsorbent [35]. Biochar is the product obtained when biomass waste is thermally treated in an anaerobic or low-oxygen environment [36]. The potential of biochar as a low-cost adsorbent for remediating steroid contamination in aqueous systems has been considered because of its large specific surface area, high porosity, and high physicochemical stability [37]. Many researchers have reported the use of biochar in the treatment of emerging contaminants (ECs) in water [38]. However, due to the limitations associated with the use of raw biochar, such as low adsorption capacity, limited adsorption range, and other defects, the biochar must be modified to enhance its removal efficiency.

There are several reports on the removal of ECs from water using modified biochar via acid–base modification [39], metal oxide and metal salt modification [40], clay mineral modification, and ball milling [38]. The ball-milling method is an emerging modification method to improve the EC adsorption capacity of biochar. The physicochemical features of biochar, such as pore size and specific surface area, can be greatly improved by the ball-milling method, which increases adsorption ability [41].

Even though ball milling is a green modification approach, not many studies have investigated the application of ball milling for the modification of pristine biochar for the simultaneous removal of the mixture of six steroidal hormones and three heavy metals. These heavy metals [42] and steroid hormones are present in different water systems, including rivers and wastewater [14,42]. According to a report [14], there was more than one steroid hormone in an effluent sample from a South African WWTP. Therefore, it is vital to find effective methods for the simultaneous removal of multiple steroid hormones and heavy metals from the wastewater before WWTP effluents are released into the environment.

Most of the works that focus on the simultaneous removal of steroidal hormones and heavy metal contaminants study the removal of one or two mixtures of the two classes of contaminants.

To the best of the author's knowledge, there is no report on ball-milled biochar derived from sweet prickly pear waste for the removal of groups of steroid hormones from an aquatic environment. Therefore, the overall aim of this work was to synthesise, characterise, and study the adsorptive performance of nano-sized, ball-milled biochar for the removal of a group of steroid hormones and heavy metals from real wastewater matrices.

2. Materials and Methods

2.1. Materials

All chemical reagents used in this work were of analytical grade and were purchased from Sigma-Aldrich (Steinheim, Germany): estriol ($C_{18}H_{24}O_3$, 97% purity, molec-

ular weight of 288.38 g/mol); β-oestradiol ($C_{18}H_{24}O_2$, 98% purity, molecular weight 272.38 g/mol); α-oestradiol ($C_{18}H_{24}O_2$, 98% purity, molecular weight 272.38 g/mol); testosterone ($C_{19}H_{28}O_2$, 99% purity, molecular weight 288.42 g/mol); progesterone ($C_{21}H_{30}O_2$, 99% purity, molecular weight 314.46 g/mol); and bisphenol A ($C_{15}H_{16}O_2$, 99% purity, molecular weight 228.29 g/mol). All the stock solutions were prepared by dissolving 10 mg of each standard in a 10 mL standard flask containing 1 mL of 50/50 methanol and ultrapure water (18.2 Ω/cm) and made up to the mark. A dilution formula was used to obtain various concentrations of the standards by diluting the stock solutions, namely cadmium nitrate $Cd(NO_3)_2 \cdot 4H_2O$, lead nitrate $Pb(NO_3)_2$, and nickel nitrate $Ni(NO_3)_2 \cdot 6H_2O$. Metal stock solutions of 1000 mg/L were prepared by added precisely weighed masses of each constituent to a 250 mL volumetric flask and filling it up to the mark using ultrapure water. To avoid metal ion hydrolysis, the standard stock solution was moderately acidified. For additional tests, working standard solutions were made by diluting the standard stock solutions with ultrapure water. The pH of the standard solutions was controlled by adding solutions of 0.1 M NaOH or HNO_3. Measurement was performed using an analytical balance (Mettler Toledo, Model AG204, Zurich, Switzerland) with a precision of 0.0001 g.

2.2. Adsorbent Preparation

The feedstock used in this study was sweet prickly pear fruit waste obtained from a local market situated in Discovery, Roodepoort, South Africa. The seeds were washed with ultrapure water, air-dried at room temperature, and stored in an airtight pack before pyrolysis. The biochar utilised in this research was derived from sweet prickly pear fruit seeds according to the method reported in [43]. Pyrolysis of a known amount of the sample was performed at a temperature of 400 °C, 500 °C, or 600 °C at a heating rate of 10 °C/min for one hour. The black solid residue obtained was ground by mortar and pestle to obtain dried biochar of small particle size. The biochar was labelled by its pyrolysis temperatures, B400, B500, and B600, before characterisation and further modification. The biochar produced by pyrolysis was further modified via the mechanochemical method using a Retsch MM 200 mixer mill machine (Verder Scientific Pty Ltd., Johannesburg, South Africa). A 1.2 g sample of each biochar (B400, B500, and B600) was weighed into each ball-milling jar (80 mL) containing 120 g beads (balls) in the ratio of 1:100 biochar/ball by mass [44]. The rotational speed was set at 550 rpm for a total milling time of 6 h with the rotational direction changed every 2 h, and the ball-milled biochar thus obtained was labelled as BMB400, BMB500, and BMB600, respectively.

2.3. Adsorbent Characterisation

The surface area, pore volume, and pore size of the biochar were determined using Brunauer–Emmett–Teller (BET) analysis with Micromeritics® ASAP™ 2020 with TriStar™ II version 2.00 software (Micromeritics Instrument Corporation, Norcross, GA, USA). The crystallinity of the biochar was analysed using X-ray powder diffraction (Rigaku SmartLab X-ray diffractometer (XRD) with Cu Kα radiation (wavelength λ = 0.154 nm) (Rigaku Corporation, Tokyo, Japan). The surface functional groups present on the biochar were identified using Fourier transform infrared (FTIR) spectroscopy (4000–400 cm^{-1} wave number) (Vertex 70v FT-IR Spectrometer, Bruker Optics, Billerica, MA, USA). An energy-dispersive spectrometer and a scanning electron microscope (SEM) were used to analyse the surface morphology, structure, and elemental content of the biochar. The SEM used was a JEOL JSM-IT 300 SEM (JEOL Ltd., Tokyo, Japan) with an Oxford Instruments EDS system (Oxford Instruments, Abingdon, Oxfordshire, UK). Thermogravimetric analysis (TGA) was carried out to determine the characteristics and thermal properties of the samples using the TGA/DSC SDT Q600 instrument (TA Instruments, New Castle, DE, USA). The thermogravimetric characteristics of the biochar were determined at a heating rate of 20 °C/min. An X-ray photoelectron spectrometer (XPS) (Thermo Fisher Scientific™ X-ray Photoelectron Spectrometer [XPS], Waltham, MA, USA) was used to determine the elemental composition and oxidation states of elements at the surface of the biochar. Raman

spectra of the biochar were obtained to identify molecules and to study chemical bonding using a confocal Raman microscope (XploRA^{TM} Plus, Horiba Scientific, Kyoto, Japan) with a laser energy of 2.411 Ev.

2.4. HPLC Separation

In this study, an Agilent 1260 Infinity HPLC-DAD system (Agilent Technologies, Waldbronn, Germany) was used for the separation of analytes. The Agilent 1260 Infinity HPLC-DAD system (Agilent Technologies, Waldbronn, Germany) used consisted of a binary pump, autosampler, diode array detector, fluorescence and refractive index detectors, and thermostat column compartment. The instrument was controlled, and data were processed by using ChemStation (version 1.9.0) software. The steroid hormones were separated using an XTerra MS C18 column (4.6 mm × 100 mm, 3.5 m) (Waters Corporation, Milford, MA, USA) at 40 °C with a mobile phase of water (solvent A) and methanol (solvent B), with a detection wavelength of 270 nm and a flow rate of 0.3 mL/min. The system was equilibrated for at least 2 min before the subsequent injection.

2.5. Batch Adsorption Experiment

The removal of steroidal hormones by pristine and ball-milled biochar was first assessed by trial experiments to determine the biochar with the highest removal efficiency. Briefly, the removal efficiency of pristine biochar (B400, B500, and B600) and that of the modified biochar by ball milling (BMB400, BMB500, and BMB600) was examined by mixing 20 mg of biochar into a 25 mL solution of 2 mg/L mixed steroidal hormones and heavy metals under given conditions (temperature = 25 °C, pH = 7.0, contact time = 60 min). After the adsorption experiment, a PVDF syringe filter with 0.45 μm pore size and a 25 mm size was used to filter the solutions. The supernatants were put into HPLC and ICP-OES (Agilent Technologies 700 series ICP-OES, Melbourne, Australia) sample bottles for analysis. Three duplicates of each experiment were run, and the average results were recorded. A factorial design was used to identify four factors that affect the current study out of the factors reported in the literature. Further optimisation using composite central design (CCD) with four-level factors generated 31 different experiments based on the factors used: pH (2–14), contact time (7.5–37.5 min), temperature (10 °C–50 °C), and varying concentrations of the contaminants (0.75–4.5 ppm). The mixtures were then filtered using a PVDF syringe filter with a 0.45 μm pore size and a 25 mm size. The filtrates were poured into HPLC and ICP-OES containers and then examined. Three duplicates of each experiment were performed, and the average results were recorded. The optimal adsorption parameters were used to obtain the adsorption data which were used for the Langmuir and Freundlich adsorption isotherm model.

$$\frac{C_e}{q_e} = \frac{1}{q_{max}b} + \frac{C_e}{q_{max}} \tag{1}$$

where q_{max} (mg g^{-1}) denotes the maximum adsorption capacity and b (L mg^{-1}) denotes the Langmuir constant for adsorption energy.

$$R_L = \frac{1}{1 + bC_o} \tag{2}$$

where C_o is the initial media concentration and b is the Langmuir constant. If $R_L < 1$, adsorption is favourable, but $R_L > 1$ indicates unfavourable adsorption, and $R_L = 0$ indicates an irreversible process.

$$\log(q_e) = \log K_f + \frac{1}{n}\log(C_e) \tag{3}$$

where Ce is the adsorbate at the equilibrium concentration (mol L^{-1}), q_e represents the quantity of adsorbate absorbed per gram at the equilibrium concentration (mg g^{-1}), K_f is the Freundlich constant which represents the adsorption capacity of the adsorbent [45]

and the strength of the adsorptive bond, and n represents the adsorption intensity of the adsorbent. The value of n indicates the ease with which the adsorption process occurs.

2.6. Optimisation by Central Composite Design (CCD)

After using factorial design to identify the factors with important effects, further optimisation was carried out to evaluate response surface methodology (RSM) using CCD with the four most important factors previously identified by factorial design: initial steroidal hormone (SH) and heavy metal (HM) concentration, pH, temperature, and contact time.

2.7. Regeneration Experiment

To determine the regeneration of the ball-milled biochar adsorbent, adsorption–desorption experiments were carried out. The ball-milled biochar used for the simultaneous removal of the six steroidal hormones (estriol, β-oestradiol, α-oestradiol, testosterone, progesterone, and bisphenol A) and heavy metals (nickel, cadmium, and lead) was desorbed using ethanol solution (10 mL) and deionised water (10 mL) at ambient temperature. After desorption, the adsorbent was filtered and dried at 353 K, and the final adsorbent was retained for reuse. In each cycle of the adsorption–desorption test, the recycled ball-milled biochar was added to 25 mL of 2 mg/L mixed solutions of the steroidal hormones. The adsorption process was then repeated five times to assess the efficiency of the regenerated ball-milled biochar [46,47].

3. Discussion of Results

3.1. Characterisation

3.1.1. BET of the Pristine and Modified Biochar

The surface properties of the adsorbents (pristine and ball-milled biochar) were assessed by BET analysis as shown in Table 1. The surface areas of biochar-based adsorbents that were produced were temperature-dependent. The surface area of biochar increased with the increase in pyrolysing temperature. The pristine biochar pyrolysed at 400 °C (B400) had a surface area of 53.1 m^2/g, which increased to 220.1 m^2/g for the pristine biochar pyrolysed at 500 °C (B500). The biochar obtained at a temperature of 600 °C (B600) possessed the largest surface area of 278.6 m^2/g. The significant increase could be attributed to the increase in the pyrolysis temperature of the biochar, which resulted in the opening of pores of the carbon and other mineral contents in the material [48]. The pristine biochar had a larger grain size than the ball-milled biochar. The ball-milling process significantly reduced the grain size of pristine biochar from 112.9 nm to 16.9 nm; this was due to the high-energy impact of balls with the biochar in the jar during the ball-milling process. The surface area of the ball-milled biochar BMB400 275.9 m^2/g increased five times in comparison to that of the pristine biochar B400 with an SA of 53.1 m^2/g. The pore volume of ball-milled biochar BMB500, 0.097 cm^3/g, was also found to be five times higher than the pristine biochar pyrolysed at 500 °C (B500) 0.021 (cm^3/g). This demonstrated that the solvent-free modification method (ball-milling) enhanced the grains' interior surface area by widening the internal porosity and increased the outer surface area by reducing the grains' particle size [49]. Furthermore, in Figure 1, a type I adsorption isotherm curve was seen in the ball-milled biochar adsorbent, indicating the development of meso- and macropores in the adsorbent. Furthermore, the porous diameter and porous volume distribution of the ball-milled biochar were predominantly mesoporous, falling within the range of 2–50 nm, with an average pore diameter of 5.6 nm and porosity of 0.097 (cm^3/g) for BMB500 [50].

3.1.2. XRD Analysis

X-ray diffraction (XRD) was used for studying biochar to determine whether the material was crystalline or amorphous. Figure 2 shows the XRD patterns of the pristine and ball-milled biochar obtained from heating biomass for 1 h at a temperature of 400, 500, or 600 °C. The raw samples were burnt in a furnace at temperatures of 400 °C, 500 °C, and 600 °C. The XRD analysis was performed for the selected samples to identify whether

substances with an amorphous or crystalline nature were formed at different combustion temperatures. A qualitative assessment of the partial crystallinity of the pristine biochar samples could be obtained from the intensity of the narrow reflections of B400, B500, and B600 in comparison to the broad band at around $2\theta = 28°$. The peak between 2θ 40°–50° corresponds to nanographene structures which are commonly present in carbon materials as well as in biochar material [51].

Table 1. Surface properties of pristine and ball-milled biochar.

| Adsorbent (Pristine and Ball-Milled Biochar)	Surface Area S_{BET} (m^2/g)	BJH Pore Volume (cm^3/g)	BJH Pore Size (nm)	Grain Size of Pristine and Ball-Milled Biochar (nm)
B400	53.1	0.003	4.7	112.9
B500	220.1	0.021	3.5	27.3
B600	278.6	0.074	5.6	21.5
BMB400	275.9	0.075	5.0	21.7
BMB500	354.6	0.097	5.6	16.9
BMB600	311.6	0.088	3.7	19.3
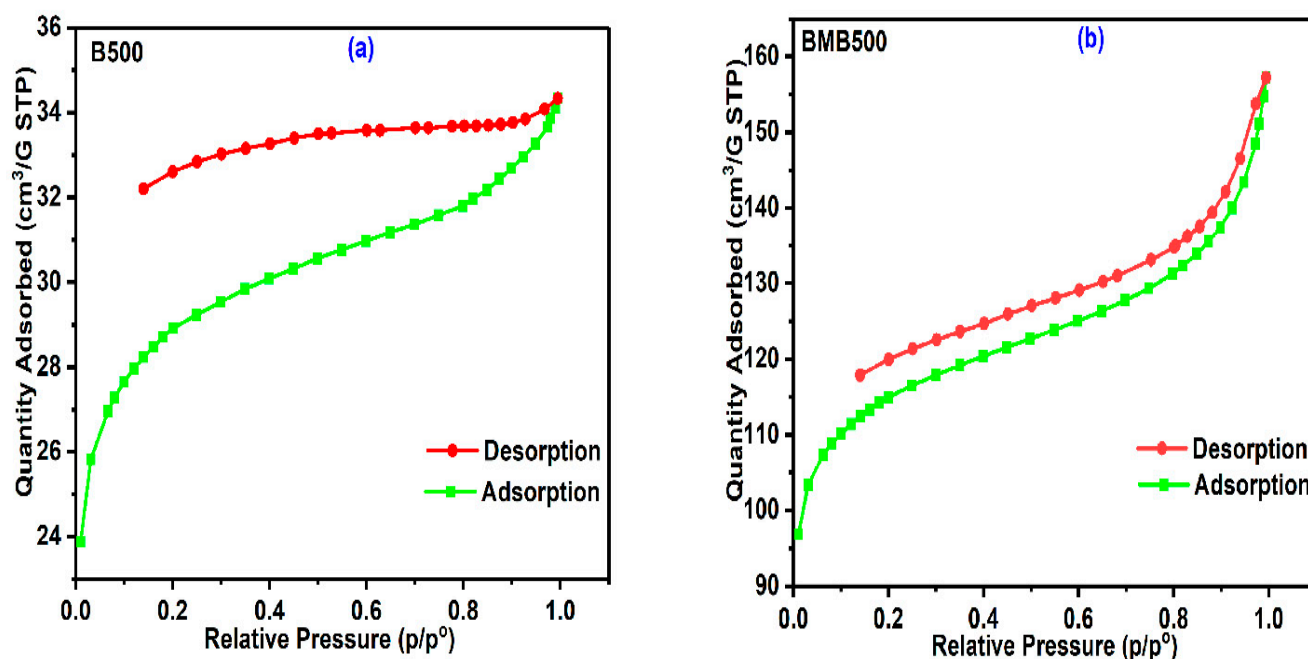
Figure 1. Isotherm curves for the adsorption and desorption of (**a**) B500 and (**b**) BMB500.

The ball-milled biochar samples (BMB400, BMB500, and BMB600) showed a strong broad peak, indicating the completely amorphous nature of the ball-milled biochar. The samples contained typically disordered carbons with high carbon content, as could be seen clearly by the broad reflections in the 2θ range from 20° to 30° in the spectra of pristine and ball-milled biochar [52].

3.1.3. FTIR Spectroscopy Analysis

The FTIR spectra in Figure 3 revealed the existence of numerous peaks that were present in all biochar samples, both pristine and ball-milled biochar. The aliphatic C-H stretching vibration was linked to one of these peaks, which appeared at 2920 cm^{-1} [53]. The carbon–carbon double bond of the aromatic group was attributed to the intensity band at 1620 cm^{-1} [54]. The peak at 1580 cm^{-1} was assigned to C=O stretching and aromatic C=C vibrations [55]. At 1080 cm^{-1}, the biochar showed a clear peak that was possibly

related to the stretching of the C-O bond [56]. An out-of-plane deformation caused by aromatic C-H atoms is indicated by the peak at 875 cm^{-1} [57].
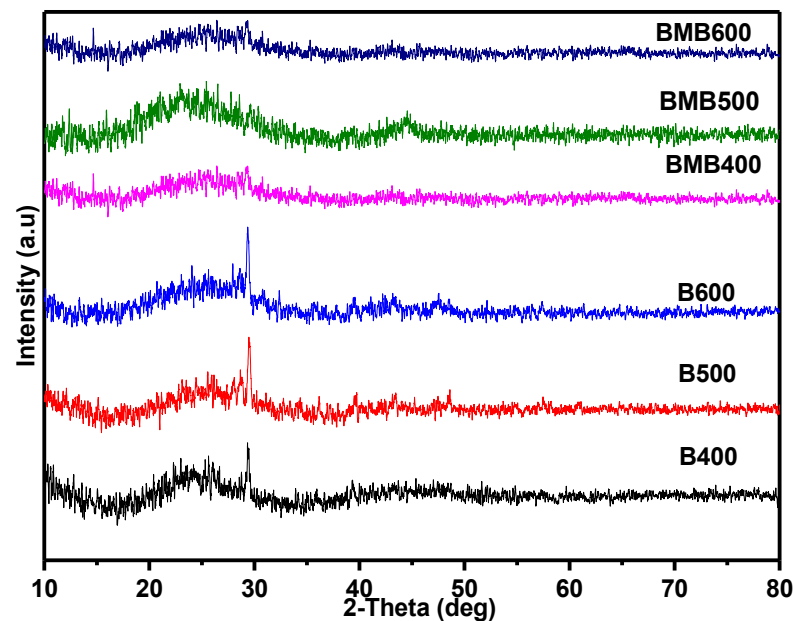
Figure 2. XRD patterns of pristine and ball-milled biochar obtained at 400, 500, and 600 °C.
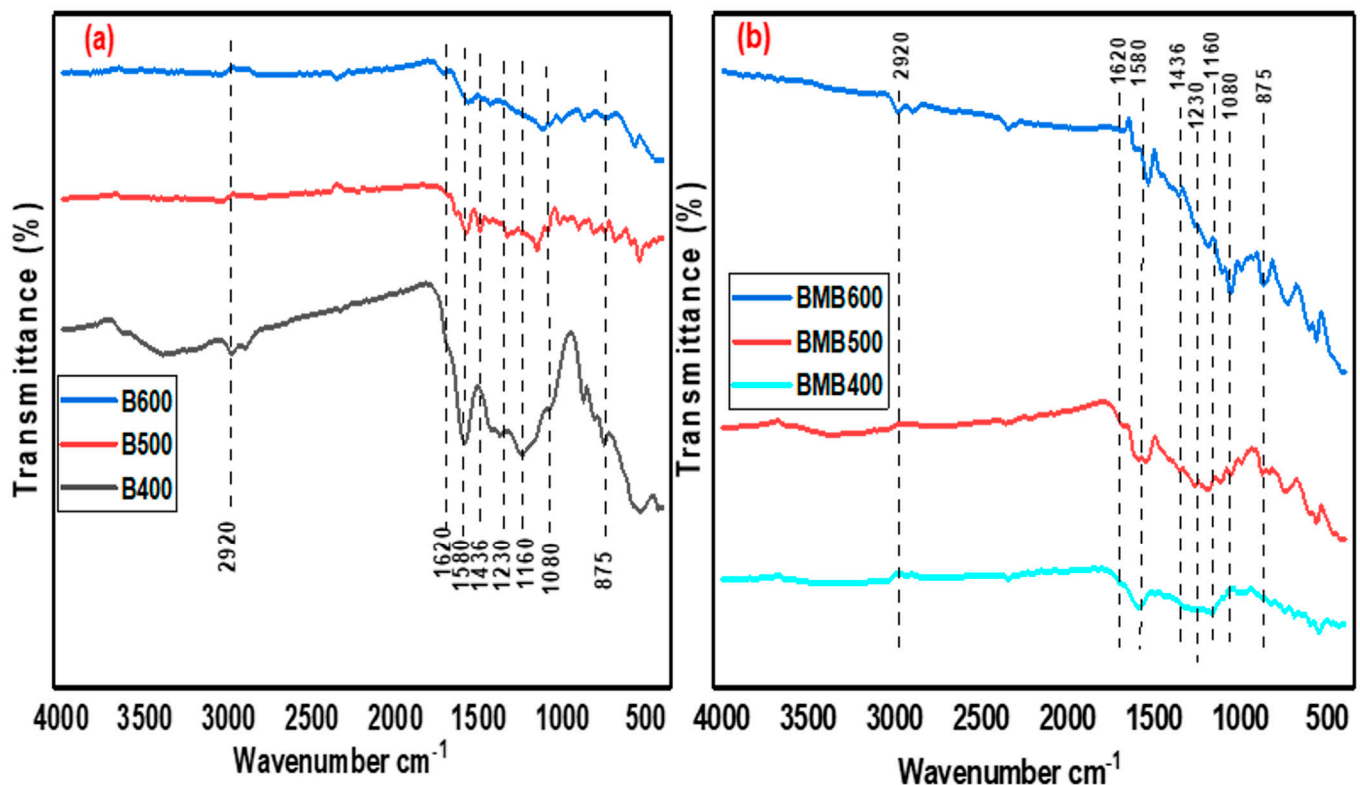
Figure 3. FTIR spectra of (**a**) pristine and (**b**) ball-milled biochar.

3.1.4. SEM and EDS Mapping

The textural characteristics and surface morphology of the pristine and ball-milled biochar were examined using 6010 PLUS/LA-JEOL-SEM equipment coupled with an Oxford EDS (Rikagu, Tokyo, Japan). Before analysis, the samples were spray-coated with gold. Figures 4 and 5 depict the morphology of the pristine and ball-milled biochar. Biochar

had a porous structure and irregularly formed particles, as seen in the SEM images in Figure 4. The substantial loss of volatile organic material during pyrolysis resulted in the formation of deep porous channels in the biochar. After ball-milling the biochar, it was apparent that the particle size had reduced, which improved the average surface area per unit volume. The average surface area (BET) and pore volume of pristine biochar (B500) and ball-milled biochar (BMB500) were 220.1 m^2/g and 0.021 cm^3/g and 354.6 m^2/g and 0.097 cm^3/g, respectively. One of the most significant aspects of bio-adsorbent research is the absorbent's high surface area. The SEM micrograph of the ball-milled biochar (BMB500) sample revealed severe agglomerates, as observed in Figure 5, which could explain its considerable surface area even with the lowest particle size. As a result, the fracture process during ball milling influenced surface area by increasing the exterior surface area as particle size decreased. The surface functional groups of biochar were also changed during the ball-milling process under different atmospheres, as was the morphology. After the ball-milling process, the oxygen content of pristine biochar (B500) increased as evident in Figure 6c,d. The oxygen content of pristine biochar was 11.0% and 14.1% after ball milling. A similar result has also been reported previously by other researchers [58].
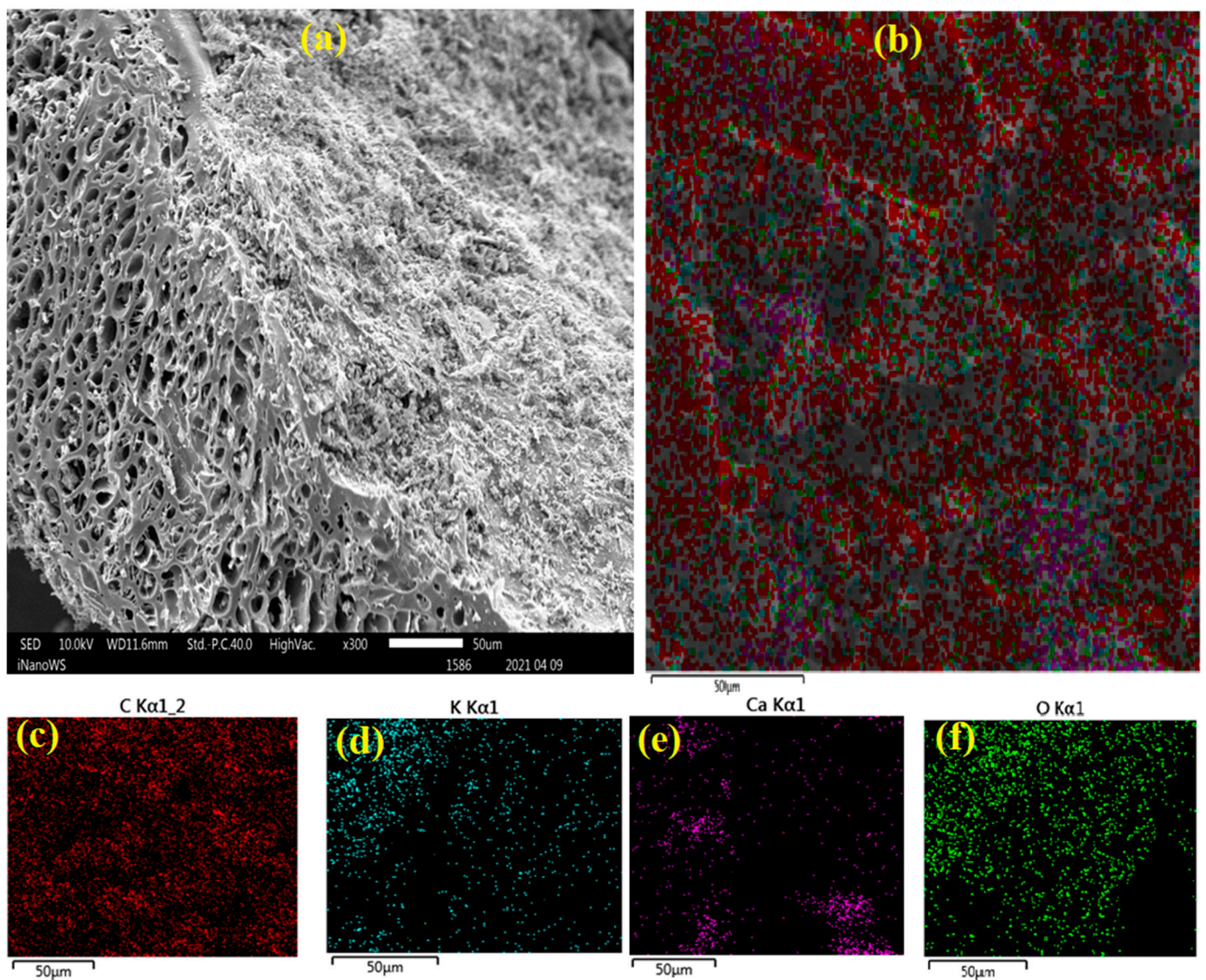

Figure 4. SEM and mapping micrograph of B500, (**a**) SEM image at 300× magnification, (**b**) full-scan mapping of all elements, (**c**) C, (**d**) O, (**e**) K, (**f**) Ca.
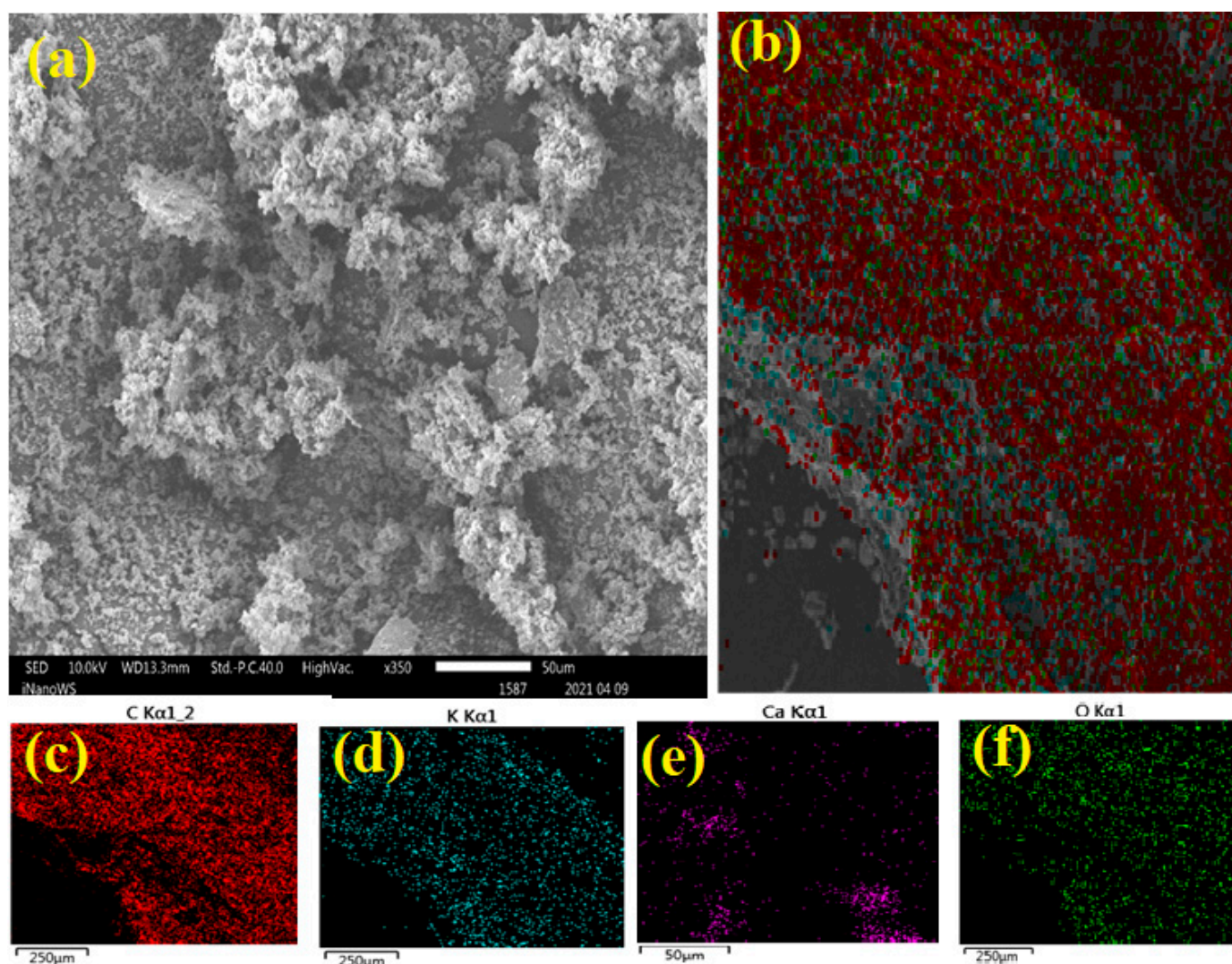
Figure 5. SEM and mapping micrograph of BMB500 (**a**) SEM image at $300\times$ magnification, (**b**) full-scan mapping of all elements, (**c**) C, (**d**) O, (**e**) K, (**f**) Ca.

3.1.5. TGA Studies

Figure 7 depicts the thermal stability of the ball-milled biochar (BMB500). Thermogravimetric analysis was carried out using the TGA-DSC SDT Q600 thermogravimetric analyser (TA Instruments, New Castle, DE, USA). A total of 10 mg of ball-milled biochar was continuously heated at a heating rate of 20 °C/min in the presence of nitrogen gas. The biochar was heated to 800 °C. Figure 7 shows the TGA results; at temperatures between 20–150 °C, there was 2% weight loss, which can be attributed to the water and other volatile organic components in biochar. We observed 11% weight loss at temperatures of 150–250 °C and 35% weight loss at temperatures between 490 and 800 °C with no significant changes in mass observed after this point [59]. A further discrepancy in the estimated stability can be seen in Figure 7, where weight loss was observed as the temperature increased. In the second curve on the graph, which represents the DSC curve, two peaks were observed, both of which corresponded to endothermic reactions. At a temperature of 20–150 °C, the first exothermic reaction took place, which had a peak at 50 °C. At a temperature of 550 °C, the second exothermic process occurred with the peak temperature at 600 °C. Both thermal approaches resulted in significant weight loss. It should be emphasised, however, that the adsorbent (BMB500) was viable over a broad range of temperatures, covering our study conditions.
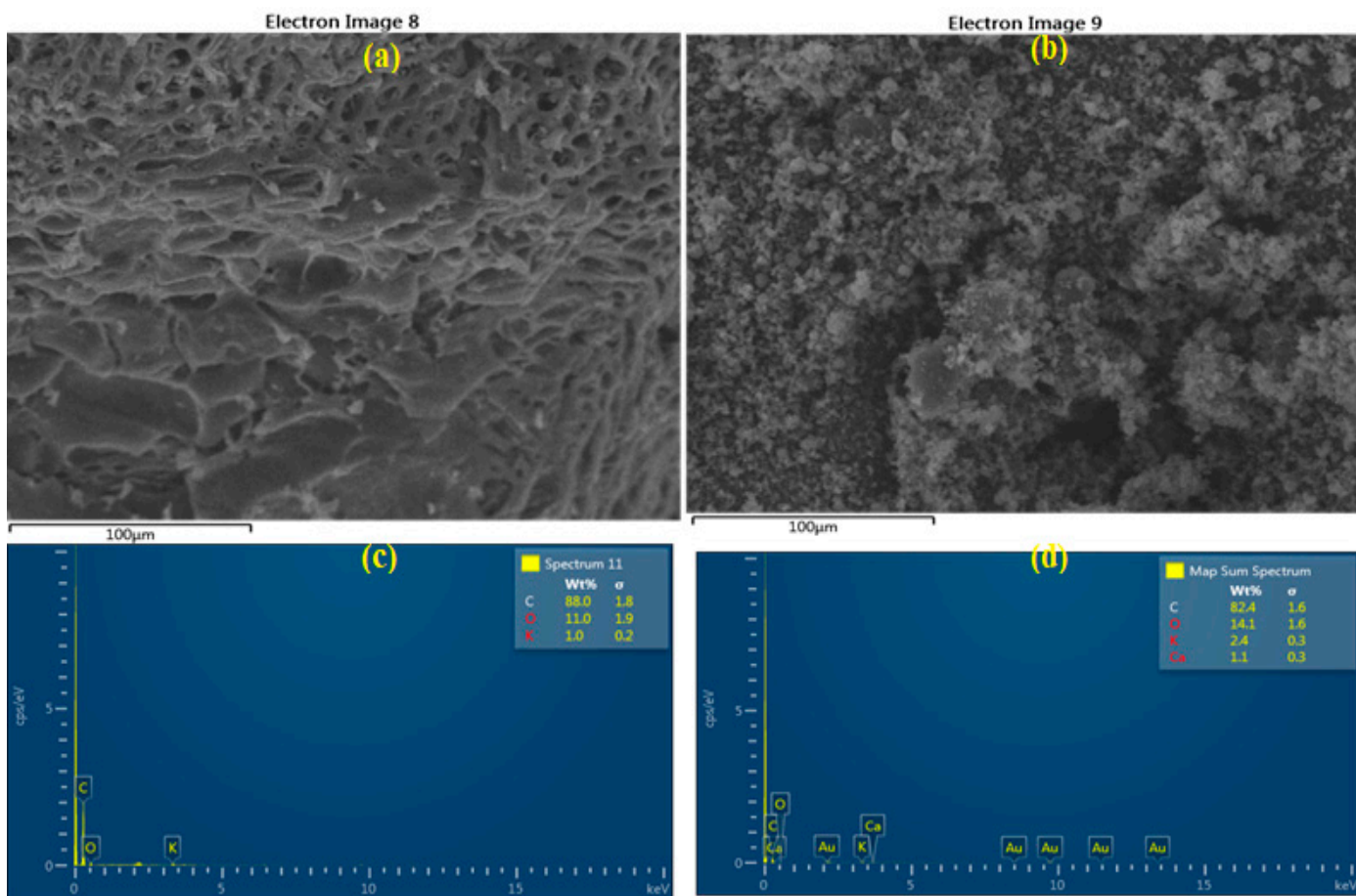
Figure 6. SEM-EDS micrograph images of B500 (**a**,**c**) and BMB500 (**b**,**d**).
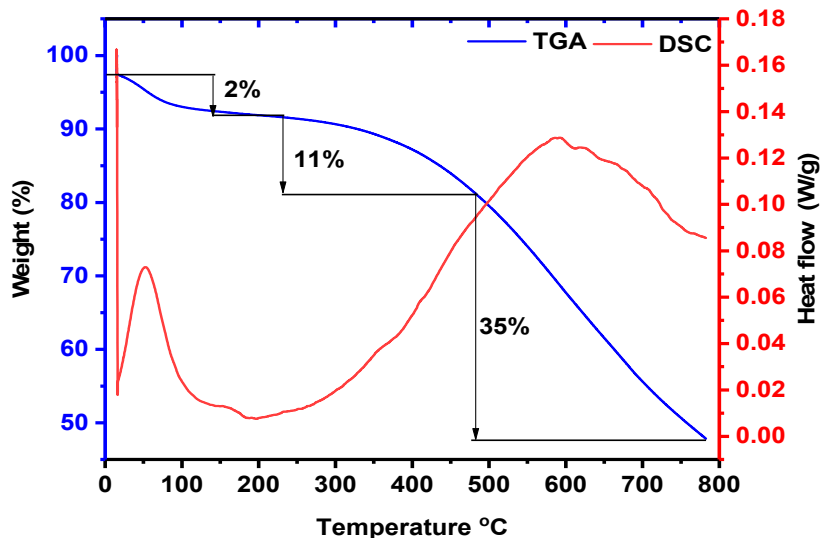
Figure 7. TGA and DSC of the BMB500.

3.1.6. XPS Analysis of Pristine and Ball-Milled Biochar

The elemental compositions of pristine and ball-milled biochar with their respective percentages of occurrence and their oxidational states with respective chemical bonds are shown in Figure 8. Figure 8a represents the full-survey scan of pristine biochar, which revealed the presence of carbon and oxygen elements. The expanded C1s for pristine biochar spectrum denotes the five peaks at C1 (284.1 eV), C2 (284.7 eV), C3 285.8 eV), C4

(287.6 eV), and C5 (288.8 eV), which were used for a deeper comprehension of the XPS spectra in Figure 8b. The C–C/C=C of amorphous carbon is seen at 284.1 eV and 284.7 eV. The Sp^2 carbon (C-O and C=O) hydroxyl and epoxy eV were attributed to peaks at 285.8 eV and 287.6 and peaks at 288.8 eV representing the carboxyl group [60]. Figure 9a shows the full-survey scan for the XPS spectra of the ball-milled biochar; similar functional groups to those of the pristine biochar were found in the expanded peak of the C1 spectrum in Figure 9b. Furthermore, the expanded spectrum of oxygen for pristine biochar (Figure 9c) denotes the peak O1. The peak of 531.4eV denotes carbonyl oxygen in carboxylic and anhydride, and the peak around 532.8 eV denotes the hydroxyl groups [61]. While there was an increase in the oxygen content of the ball-milled biochar from 14.8% to 21.5%, this could be attributed to the effect of ball milling, as it has been reported that ball milling can induce oxygen functional groups (moieties) on the surface of ball-milled biochar [62]. The expanded O1 peak of ball-milled biochar shown in Figure 9c depicts carbonyl oxygen at 529.9 eV; carbonyl oxygen in carboxylic and anhydride forms at around 531.7 eV, as well as oxygen atoms in hydroxyl groups; and non-carbonyl (ether-type) oxygen in esters and anhydrides at 533.3 eV [63].
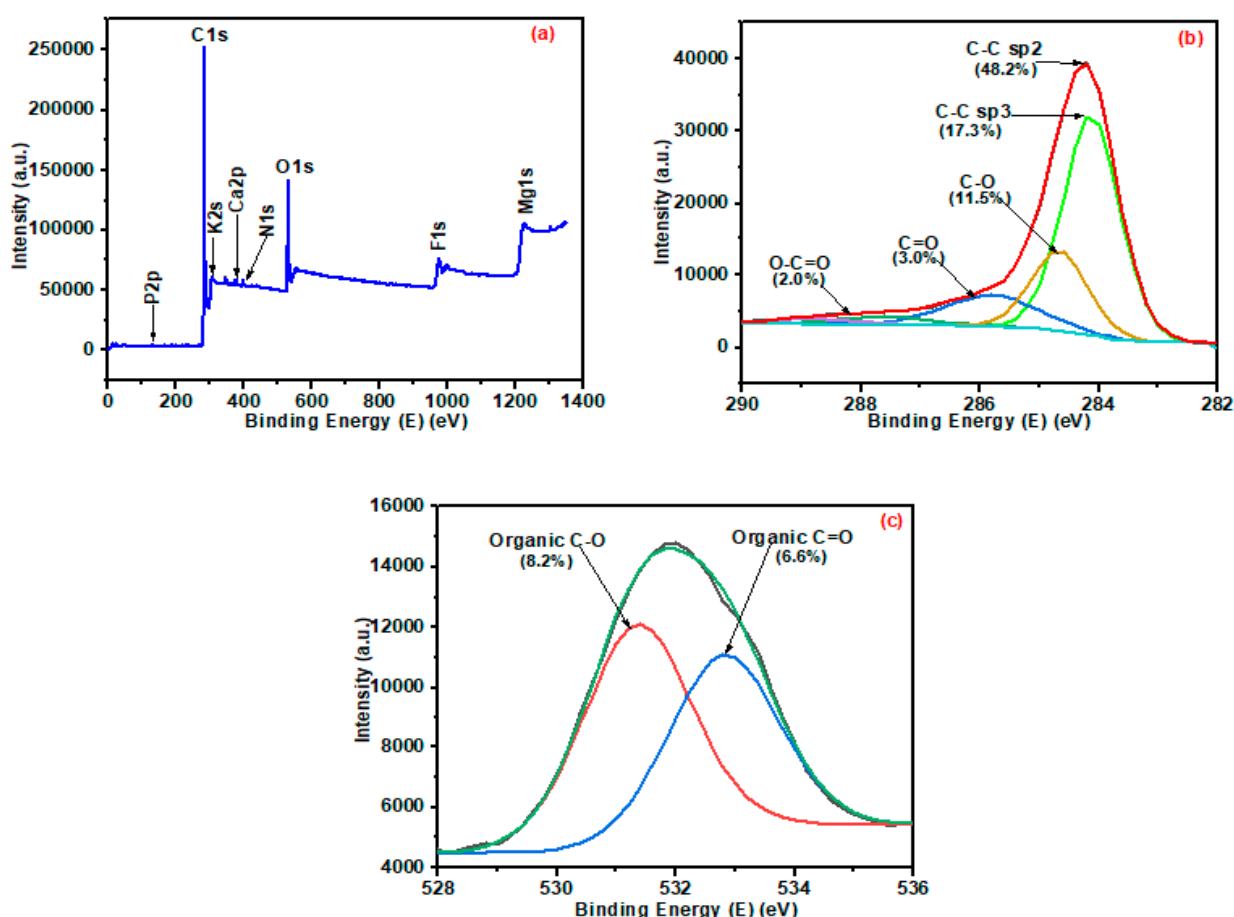
Figure 8. (**a**) Full-survey scan, (**b**) carbon and (**c**) oxygen element spectra of B500.

3.1.7. Raman Spectroscopy Analysis

Figure 10 shows the Raman spectra of pristine biochar (B500) and ball-milled biochar (BMB500). The spectra of the B500 and BMB500 showed two separate well-defined bands, which are popularly referred to as the D and G bands. The in-plane resonance of the sp2 hybridised carbon atoms (G band) and the sp3 carbon atoms of disorderly graphite (D band) was ascribed at 1350 and 1580 cm^{-1} [64]. After ball-milling, the intensity of the D and G bands in pristine biochar was lowered, which could be due to disorder in the c axis and the development of high specific surface area structures; this is related to crystal

size [65]. High-energy ball-milling processes could readily alter the original ordering of the basal planes and perhaps even reduce huge starting crystals to extremely tiny sizes during the milling process because the structure of the amorphous phase produced by ball milling is less disordered [66].
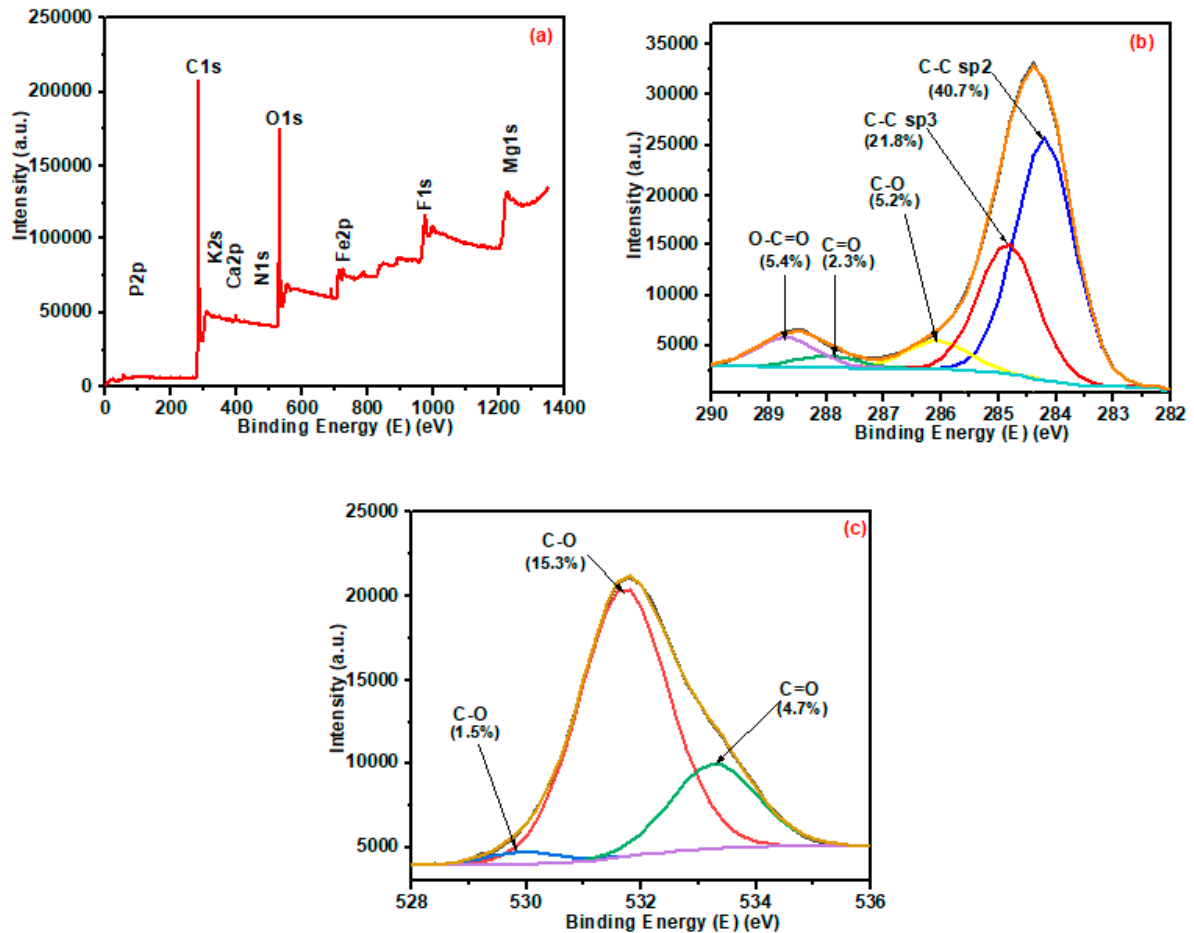

Figure 9. (**a**) Full-survey scan, (**b**) carbon and (**c**) oxygen spectra of BMB500.
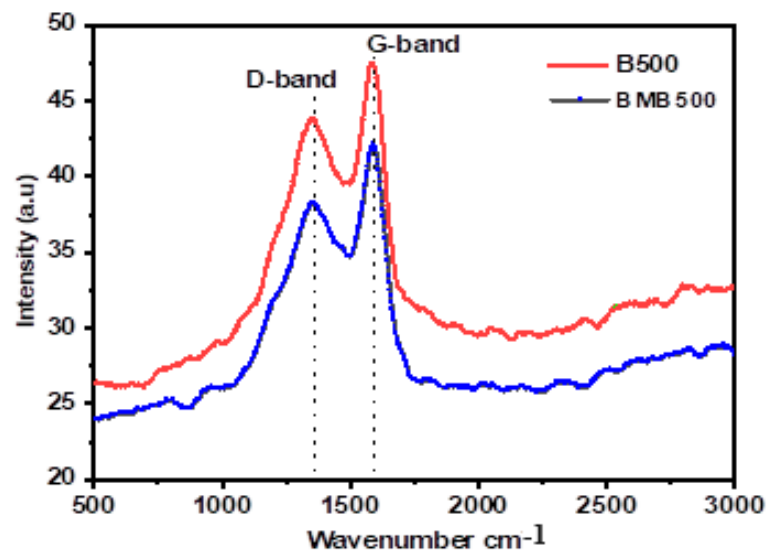

Figure 10. Raman spectra of B500 and BMB500.

3.2. Adsorption Experiments

Adsorption Isotherm

The use of experimental data from adsorption processes to model the mechanisms of various adsorption systems is a highly significant method for predicting the mechanisms of different adsorption systems [67]. Langmuir and Freundlich isotherms are frequently used linear isotherm equations often employed to determine the best-fit isotherm for all the adsorbates under study. The Langmuir equation may be expressed in linear form as given in Equation (1) [68].

The quantity of steroidal hormones and heavy metals adsorbed at the equilibrium concentration is q_e (mg g^{-1}) and the equilibrium concentration of adsorbate is C_e (mol L^{-1}). A similar correlation was seen when $\frac{C_e}{q_e}$ was plotted against C_e, as given in the Supplementary Materials. The Langmuir separation factor (R_L) is a dimensionless constant that expresses the important attributes of the Langmuir isotherm given in Equation (2) [69].

The Freundlich isotherm is used to describe multilayer adsorption on heterogonous surfaces [69]. The surface heterogeneity and the exponential distribution of active sites and their energy are defined by this isotherm [70]. The Freundlich equation may be expressed in linear form as given in Equation (3).

The adsorption intensity or surface heterogeneity is measured by n (heterogeneity factor, which ranges from 0 to 1). The empirical constants K_f and n may be calculated from the intercept and slope of a plot of log q_e vs log C_e. From the results presented in Table 2, the values of 1/n were found to be between 0 and 1, which indicates favourable adsorption of steroidal hormones and heavy metals on the surface of ball-milled biochar.

Table 2. Langmuir and Freundlich adsorption constants for adsorption of steroidal hormones and heavy metals using ball-milled biochar.

Analyte	Langmuir				Freundlich		
	q_{max} (mg g^{-1})	b (L mg^{-1})	R_L	R^2	K_f (L mg^{-1})	1/n	R^2
Estriol	14.53	0.2464	0.4742	0.9840	7.70	0.4547	0.9941
α-Oestradiol	10.58	0.2743	0.4475	0.9759	5.32	0.3585	0.9843
β-Oestradiol	12.50	0.3060	0.4207	0.9924	7.79	0.5014	0.9754
Testosterone	5.73	0.6955	0.2421	0.9238	5.51	0.5169	0.9919
Progesterone	5.63	0.6199	0.2639	0.9724	5.11	0.5108	0.9998
Bisphenol A	9.75	0.3400	0.3953	0.9929	6.56	0.5206	0.9546
Nickel	8.58	0.2957	0.2483	0.9888	4.12	0.5263	0.9768
Cadmium	4.15	0.7615	0.2589	0.9974	5.75	0.6289	0.7845
Lead	6.95	0.7542	0.2568	0.9884	3.54	0.7142	0.8692

Based on the results, both Freundlich and Langmuir isotherm models fit the adsorption data very well. However, from the correlation coefficient values (R^2) obtained, the Freundlich isotherm shows a higher correlation coefficient value for steroidal hormones, but the Langmuir isotherm shows a higher correlation coefficient for heavy metals (Table 2). This might be the case because the removal of steroidal hormones was accomplished using low solution concentrations, which led to the Freundlich isotherm having the best fit, and the removal of heavy metals was accomplished using high-concentration metal ions solutions, which led to the Langmuir isotherm having the best fit. The results suggest that steroidal hormones were adsorbed on multilayer heterogenous surfaces, whereas heavy metals were adsorbed on monolayer surfaces at a finite number of active sites. The maximum adsorption capacities were 14.53 (mg g^{-1}), 10.58 (mg g^{-1}), 12.50 (mg g^{-1}), 5.73 (mg g^{-1}), 5.63 (mg g^{-1}), and 9.75 (mg g^{-1}) for estriol, α-oestradiol, β-oestradiol, testosterone, progesterone, and bisphenol A. For heavy metals, the maximum adsorption capacities of 8.58 (mg g^{-1}), 4.15 (mg g^{-1}), and 6.95 (mg g^{-1}) for nickel, cadmium, and lead were obtained, respectively.

3.3. CCD Modelling

The adsorbent (BMB500) was found to have the highest removal efficiency, which was also confirmed by the results obtained from the characterisation of the biochar. This biochar was chosen for further optimisation of the adsorption experiment using the factorial design in Minitab 21 statistical software. RSM based on CCD is a mathematical and statistical approach for designing experiments, evaluating the interaction between independent factors, and determining the best response synergy before assessing response patterns [71]. Initial steroidal hormone (SH) and heavy metal (HM) concentrations, pH, temperature, and contact time were investigated at five different levels: (lowest), 1 (low), 0 (mid), +1 (high), and + (highest), with the levels determined as established in previous research outcomes from factorial design for factors with the greatest effect, as well as previous studies in the literature [72,73]. Table 3 depicts the variables and levels.

$$
\begin{aligned}
\text{Estriol Removal} \quad &= 60.4 - 14.93\,\text{A} - 14.7\,\text{B} + 7.22\,\text{C} + 0.77\,\text{D} - 0.031\,\text{A} * \text{A} + 2.61\,\text{B} * \text{B} \\
&\quad -0.1050\,\text{C} * \text{C} + 0.0222\,\text{D} * \text{D} + 0.94\,\text{A} * \text{B} + 0.317\,\text{A} * \text{C} + 0.163\,\text{A} * \text{D} \\
&\quad -0.200\,\text{B} * \text{C} - 0.350\,\text{B} * \text{D} - 0.1150\,\text{C} * \text{D}
\end{aligned} \tag{4}
$$

$$
\begin{aligned}
\alpha - \text{Oestradiol Removal} \quad &= 17.1 - 14.73\,\text{A} - 7.7\,\text{B} + 8.36\,\text{C} + 2.32\,\text{D} + 0.061\,\text{A} * \text{A} + 2.53\,\text{B} * \text{B} \\
&\quad -0.1303\,\text{C} * \text{C} + 0.0005\,\text{D} * \text{D} + 0.92\,\text{A} * \text{B} + 0.297\,\text{A} * \text{C} + 0.131\,\text{A} * \text{D} \\
&\quad -0.278\,\text{B} * \text{C} - 0.475\,\text{B} * \text{D} - 0.1025\,\text{C} * \text{D}
\end{aligned} \tag{5}
$$

$$
\begin{aligned}
\beta - \text{Oestradiol Removal} \quad &= 11.6 - 16.66\,\text{A} + 2.9\,\text{B} + 8.06\,\text{C} + 2.85\,\text{D} + 0.031\,\text{A} * \text{A} - 1.51\,\text{B} * \text{B} \\
&\quad -0.1284\,\text{C} * \text{C} - 0.0072\,\text{D} * \text{D} + 1.31\,\text{A} * \text{B} + 0.319\,\text{A} * \text{C} + 0.160\,\text{A} * \text{D} \\
&\quad -0.078\,\text{B} * \text{C} - 0.442\,\text{B} * \text{D} - 0.1175\,\text{C} * \text{D}
\end{aligned} \tag{6}
$$

$$
\begin{aligned}
\text{Testosterone Removal} \quad &= 2.8 - 14.89\,\text{A} + 17.2\,\text{B} + 7.48\,\text{C} + 2.52\,\text{D} - 0.029\,\text{A} * \text{A} - 2.25\,\text{B} * \text{B} \\
&\quad -0.1358\,\text{C} * \text{C} - 0.0051\,\text{D} * \text{D} + 0.36\,\text{A} * \text{B} + 0.392\,\text{A} * \text{C} + 0.140\,\text{A} * \text{D} \\
&\quad -0.189\,\text{B} * \text{C} - 0.458\,\text{B} * \text{D} - 0.1025\,\text{C} * \text{D}
\end{aligned} \tag{7}
$$

$$
\begin{aligned}
\text{Progesterone Removal} \quad &= 17.7 - 16.42\,\text{A} + 2.9\,\text{B} + 8.82\,\text{C} + 1.62\,\text{D} + 0.050\,\text{A} * \text{A} + 1.03\,\text{B} * \text{B} \\
&\quad -0.1364\,\text{C} * \text{C} + 0.0120\,\text{D} * \text{D} + 0.89\,\text{A} * \text{B} + 0.350\,\text{A} * \text{C} + 0.154\,\text{A} * \text{D} \\
&\quad -0.422\,\text{B} * \text{C} - 0.517\,\text{B} * \text{D} - 0.1067\,\text{C} * \text{D}
\end{aligned} \tag{8}
$$

$$
\begin{aligned}
\text{Bisphenol A Removal} \quad &= 17.7 - 16.42\,\text{A} + 2.9\,\text{B} + 8.82\,\text{C} + 1.62\,\text{D} + 0.050\,\text{A} * \text{A} + 1.03\,\text{B} * \text{B} \\
&\quad -0.1364\,\text{C} * \text{C} + 0.0120\,\text{D} * \text{D} + 0.89\,\text{A} * \text{B} + 0.350\,\text{A} * \text{C} + 0.154\,\text{A} * \text{D} \\
&\quad -0.422\,\text{B} * \text{C} - 0.517\,\text{B} * \text{D} - 0.1067\,\text{C} * \text{D}
\end{aligned} \tag{9}
$$

$$
\begin{aligned}
\text{Nickel} \quad &= 70.1 - 1.63\,\text{A} - 24.6\,\text{B} - 0.032\,\text{C} + 0.377\,\text{D} + 0.128\,\text{A} * \text{A} + 3.45\,\text{B} * \text{B} + 0.00131\,\text{C} * \text{C} - 0.00006\,\text{D} * \text{D} \\
&\quad +1.44\,\text{A} * \text{B} - 0.0094\,\text{A} * \text{C} - 0.0241\,\text{A} * \text{D} - 0.003\,\text{B} * \text{C} - 0.066\,\text{B} * \text{D} - 0.00118\,\text{C} * \text{D}
\end{aligned} \tag{10}
$$

$$
\begin{aligned}
\text{Cadmium} \quad &= 68.9 - 2.33\,\text{A} - 26.1\,\text{B} + 0.035\,\text{C} + 0.322\,\text{D} + 0.160\,\text{A} * \text{A} + 3.62\,\text{B} * \text{B} + 0.00101\,\text{C} * \text{C} + 0.00048\,\text{D} * \text{D} \\
&\quad +1.53\,\text{A} * \text{B} - 0.0078\,\text{A} * \text{C} - 0.0255\,\text{A} * \text{D} - 0.007\,\text{B} * \text{C} - 0.068\,\text{B} * \text{D} - 0.00155\,\text{C} * \text{D}
\end{aligned} \tag{11}
$$

$$
\begin{aligned}
\text{Lead} \quad &= 72.7 - 2.67\,\text{A} - 26.0\,\text{B} + 0.026\,\text{C} + 0.344\,\text{D} + 0.179\,\text{A} * \text{A} + 3.49\,\text{B} * \text{B} + 0.00098\,\text{C} * \text{C} - 0.00002\,\text{D} * \text{D} \\
&\quad +1.51\,\text{A} * \text{B} - 0.0076\,\text{A} * \text{C} - 0.0241\,\text{A} * \text{D} - 0.008\,\text{B} * \text{C} - 0.057\,\text{B} * \text{D} - 0.00131\,\text{C} * \text{D}
\end{aligned} \tag{12}
$$

3.3.1. Factorial Design for Optimisation

The removal of steroidal hormones by adsorption in a batch system is generally determined by many variables. The pH of the medium, adsorbent dosage, initial steroid hormone and heavy metal concentrations, contact time, temperature, and so on are examples of these variables. When any factor is optimised, only one parameter is altered at a time while the others are kept constant; as a result, the optimal value obtained by this process is fixed while the other factors are altered one at a time. Therefore, utilising the univariate procedure to optimise all variables is highly time-intensive and increases chemical consumption. The optimal condition could not be found using the univariate method

since the interactions between all components were kept constant [74]. Batch adsorption experiments using full factorial designs were carried out by studying various degrees of factors in all possible combinations. To examine the effects as well as the statistical parameters, the findings of the experimental design were evaluated using MINITAB 21 statistical software [75].

Table 3. Factors of the independent variables and levels of the variables used to build the central composite design (CCD).

Factor	Unit	Code	Coded Actual Levels				
			Lowest	Low Level	Mid Level	High Level	Highest
			$-\alpha$	(-1)	0	$(+1)$	$+\alpha$
pH	-	A	2	5	8	11	14
Concentration	ppm	B	0.75	1.5	3	3.75	4.5
Time	min	C	7.5	15	22.5	30	37.5
Temperature	°C	D	10	20	30	40	50

$\alpha = 2$ for the CCD of the three-level factorial: full factorial.

3.3.2. Validation of the Model and Statistical Analysis

A total of 31 runs were performed following the CCD design of experiments, and the results of the statistical program and response processes are presented in Table 4. The effectiveness of removing steroidal hormones (SHs) and heavy metals (HMs) with five different levels of the four factors was shown to be significant. The maximum and minimum percentages of SH absorption by BMB500, according to the experimental CCD research, were 93% and 22%, respectively, which were achieved in experiment runs no. 24 and 30 [76]. This might be due to changes in variables, which cause diverse interactions that impact the percentage removal; consequently, they can be used to improve the clean-up process. The interaction between independent factors and response values was described using a second-order polynomial equation and a quadratic model. As a result, the regression model was well-fitted, and the efficacy of BMB500 in removing SHs for the important variables was calculated by regression equations which were in coded units for each of the hormones and heavy metals. While A is the pH of the solution, B is the concentration of the steroidal hormones and heavy metals in ppm, C is the time of the reaction in minutes, and D is the temperature of the solution in °C.

Second-order models are effective in solving practical response surface problems. Owing to their flexibility and ability to hold on to a broad range of diverse configurations, the second-order polynomial equation is a suitable interpolation approach to the genuine response in RSM [77].

Table 4. CCD design matrix for SH adsorption factors and respective responses (% removal).

Std Order	Run Order	Pt Type	pH	Conc	Time	Temp	Estriol	Alpha-Oestradiol	Beta-Oestradiol	Testosterone	Progesterone	Bisphenol A
6	1	1	11	1.50	30.0	20	90	90	91	95	92	98
17	2	−1	2	2.25	22.5	30	89	85	90	94	91	96
16	3	1	11	3.00	30.0	40	50	52	55	58	54	54
2	4	1	11	1.50	15.0	20	47	40	44	38	35	37
30	5	0	8	2.25	22.5	30	88	87	90	92	93	90
31	6	0	8	2.25	22.5	30	79	77	81	85	80	83
26	7	0	8	2.25	22.5	30	81	82	85	83	87	88
11	8	1	5	3.00	15.0	40	52	55	56	56	60	51
22	9	−1	8	2.25	37.5	30	86	85	82	86	79	86
14	10	1	11	1.50	30.0	40	80	78	79	72	75	84
8	11	1	11	3.00	30.0	20	78	79	81	85	80	81
24	12	−1	8	2.25	22.5	50	93	95	91	92	89	98
7	13	1	5	3.00	30.0	20	70	72	75	78	71	73
20	14	−1	8	3.75	22.5	30	84	82	87	82	84	87
18	15	−1	14	2.25	22.5	30	82	77	85	85	85	85
5	16	1	5	1.50	30.0	20	81	86	84	79	81	84
10	17	1	11	1.50	15.0	40	65	70	69	75	72	69
27	18	0	8	2.25	22.5	30	69	75	73	75	73	73
21	19	−1	8	2.25	7.5	30	26	32	30	33	38	30
12	20	1	11	3.00	15.0	40	60	63	61	68	54	61
19	21	−1	8	0.75	22.5	30	93	94	95	88	84	95
28	22	0	8	2.25	22.5	30	65	63	68	70	73	68
29	23	0	8	2.25	22.5	30	64	62	66	81	79	66
15	24	1	5	3.00	30.0	40	39	42	40	41	45	40
9	25	1	5	1.50	15.0	40	80	85	83	83	83	83
23	26	−1	8	2.25	22.5	10	85	87	80	79	85	89
1	27	1	5	1.50	15.0	20	80	82	79	87	83	80
3	28	1	5	3.00	15.0	20	65	67	68	70	75	68
13	29	1	5	1.50	30.0	40	83	81	87	90	83	86
4	30	1	11	3.00	15.0	20	22	20	25	22	20	23
25	31	0	8	2.25	22.5	30	75	67	75	80	78	77

3.3.3. ANOVA Analysis

To ensure that the model and variance analyses were accurate, the outcomes of the analyses were subjected to variance analysis (ANOVA). The F-test and probability of error (*p*-values) for ANOVA were employed to assess the importance of every model factor at a 95% confidence level. When the *p*-value was less than 0.05, the experimental design was significant, but *p*-values were greater than 0.1, showing that the model terms were not significant [78]. Tables 5 and 6 show the ANOVA results for steroidal hormones (SHs) and heavy metals (HMs) in the model. The model was significantly based on *p*-values, as evidenced by the *p*-value in the regression of all the SHs studied: estriol (0.037), α-oestradiol (0.017), β-oestradiol (0.015), testosterone (0.028), progesterone (0.017), and bisphenol A (0.020). Similar results were seen for HMs: nickel (0.009), cadmium (0.014), and lead (0.006). The results show that the parameters used in this study are notable or have a coordinated synergetic effect on the simultaneous removal of SHs and HMs by the ANOVA experimental design. The coefficient of the lack-of-fit assessment was designed to see if the proposed method was suitable for interpreting the observed data or if a more sophisticated model was required. If the model was not well-fitted, the test would be significant [79]. The F-value of the model for the SHs and HMs were estriol (12.56), α-oestradiol (13.07), β-oestradiol (13.14), testosterone (12.74), progesterone (13.06), bisphenol A (12.96), nickel (14.1), cadmium (14.2) and lead (13.8), indicating that all parameters were significant. The model's moderate *p*-values for lack-of-fit estriol (0.070), α-oestradiol (0.019), β-oestradiol (0.029), testosterone (0.022), progesterone (0.030), bisphenol A (0.043), nickel (0.059), cadmium (0.049), and lead (0.056) were significant, suggesting that the model was acceptable and significant in demonstrating the relationship between the component variables (pH, concentration, time, and temperature) and the response of the process (estriol, α-oestradiol, β-oestradiol, testosterone, progesterone, bisphenol A, nickel, cadmium, and lead) [80].

Table 5. CCD design matrix for HM adsorption factors and respective responses (% removal).

Std Order	Run Order	Pt Type	pH	Concentration	Time	Temperature	Ni	Cd	Pb
5	1	1	2.5	0.5	150.0	15.0	88	93	94
6	2	1	12.5	0.5	150.0	15.0	89	92	93
17	3	−1	−2.5	1.5	82.5	42.5	53	56	57
13	4	1	2.5	0.5	150.0	70.0	42	36	38
22	5	−1	7.5	1.5	217.5	42.5	89	90	95
25	6	0	7.5	1.5	82.5	42.5	78	83	82
7	7	1	2.5	2.5	150.0	15.0	83	81	89
3	8	1	2.5	2.5	15.0	15.0	55	54	62
23	9	−1	7.5	1.5	82.5	12.5	80	84	81
18	10	−1	17.5	1.5	82.5	42.5	75	70	77
19	11	−1	7.5	0.5	82.5	42.5	80	83	82
2	12	1	12.5	0.5	15.0	15.0	89	90	91
31	13	0	7.5	1.5	82.5	42.5	73	76	73
8	14	1	12.5	2.5	150.0	15.0	85	80	86
27	15	0	7.5	1.5	82.5	42.5	83	83	87
21	16	−1	7.5	1.5	52.5	42.5	82	77	83
24	17	−1	7.5	1.5	82.5	97.5	65	75	75
9	18	1	2.5	0.5	15.0	70.0	70	72	75
15	19	1	2.5	2.5	150.0	70.0	28	31	40
10	20	1	12.5	0.5	15.0	70.0	60	66	56
1	21	1	2.5	0.5	15.0	15.0	91	86	86
4	22	1	12.5	2.5	15.0	15.0	67	78	75
16	23	1	12.5	2.5	150.0	70.0	62	79	81
26	24	0	7.5	1.5	82.5	42.5	37	39	47
30	25	0	7.5	1.5	82.5	42.5	80	81	85
12	26	1	12.5	2.5	15.0	70.0	78	77	87
11	27	1	2.5	2.5	15.0	70.0	74	85	87

Std Order	Run Order	Pt Type	pH	Concentration	Time	Temperature	Ni	Cd	Pb
29	28	0	7.5	1.5	82.5	42.5	63	68	77
28	29	0	7.5	1.5	82.5	42.5	82	88	85
20	30	−1	7.5	3.5	82.5	42.5	74	20	25
14	31	1	12.5	0.5	150.0	70.0	73	78	79

The 3D surfaces and 2D contour plots for a function of two parameters are shown to examine the effects of variables. When the other variables are held constant, this diagram depicts the relative influence of any two variables. The plots of the three-dimensional response surfaces (3D) and contour curves (2D) generated to depict the major interactions are shown in Figure 11A,D,E and show the interaction of pH and concentration with removal percentages of estriol, testosterone, and progesterone, respectively. The removal of estriol, testosterone, and progesterone was greatly favoured at a slightly acidic pH and at lower concentrations of the solution. The analysis of the interactive effect of pH and time is shown in Figure 11B,C,F for α-oestradiol, β-oestradiol, and bisphenol A, respectively. The removal of BPA was favoured (Figure 11), and according to these figures, the interactions showed that the surface-response SRM plot of α-oestradiol, β-oestradiol, and bisphenol A with pH and time had an interaction effect greater than 95% when working with pH and concentration.
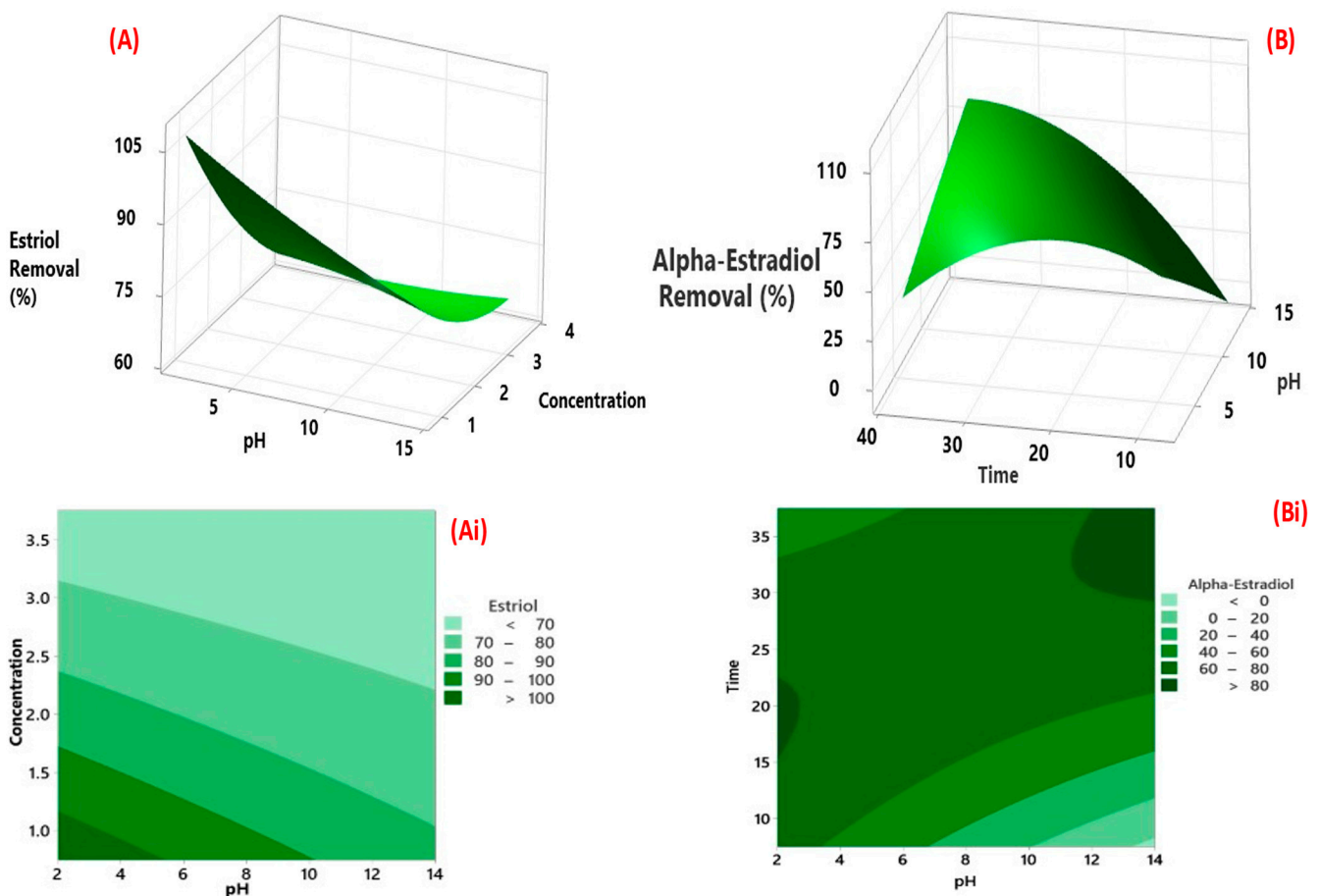
Figure 11. *Cont.*
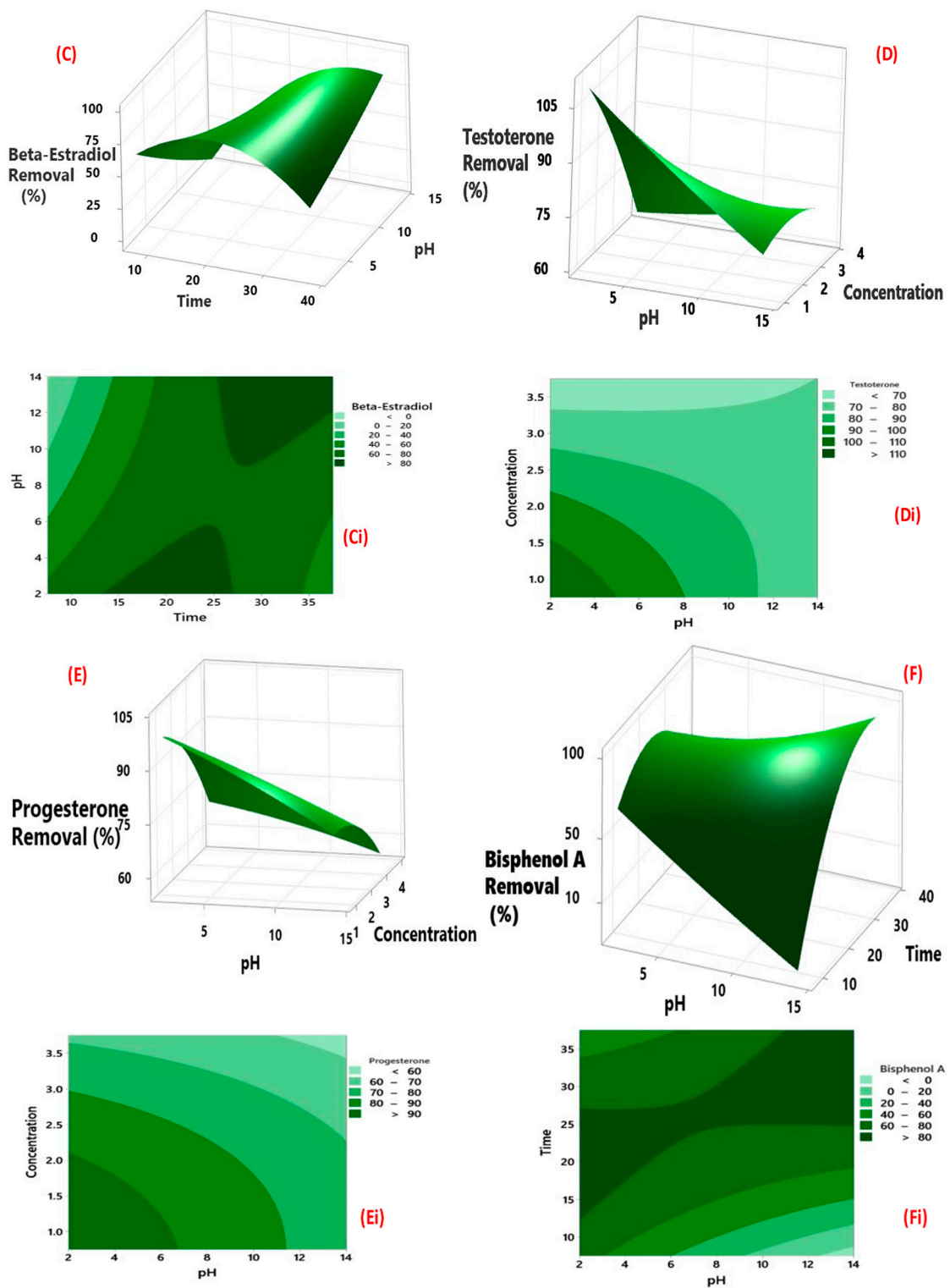
Figure 11. Three-dimensional (3D) SRM and (2D) counterplots for interaction effects of factors for SH removal by biochar.

Table 6. Results for ANOVA of various steroidal hormones (SHs) and heavy metals (HMs) in the CCD model.

Analyte Source	Estriol (Values)		α-Oestradiol (Values)		β-Oestradiol (Values)		Testosterone (Values)		Progesterone (Values)		Bisphenol A (Values)		Nickel (Values)		Cadmium (Values)		Lead (Values)	
	F	p	F	p	F	p	F	p	F	p	F	p	F	p	F	p	F	p
Model	12.5	0.037	13.07	0.017	13.1	0.15	12.74	0.28	13.06	0.017	12.96	0.020	14.1	0.009	14.2	0.014	13.8	0.006
Linear	4.58	0.012	5.11	0.008	5.03	0.008	4.00	0.020	4.14	0.017	4.82	0.009	5.4	0.017	6.4	0.039	5.8	0.016
pH	1.07	0.317	2.12	0.164	1.50	0.239	1.72	0.208	3.08	0.098	1.26	0.277	0.33	0.015	0.30	0.059	0.29	0.005
Conc	7.28	0.016	8.31	0.011	7.38	0.015	5.09	0.038	5.26	0.036	6.83	0.019	1.33	0.002	1.60	0.224	1.49	0.024
Time	9.97	0.006	10.00	0.006	11.24	0.004	9.13	0.008	8.20	0.011	11.38	0.004	0.50	0.489	0.60	0.449	0.52	0.048
Temp	0.01	0.910	0.01	0.927	0.01	0.938	0.5	0.828	0.00	0.963	0.00	0.978	0.00	0.982	0.07	0.788	0.02	0.081
Square	2.01	0.142	1.97	0.157	2.61	0,075	1.99	0.145	2.53	0.081	2.22	0.113	0.48	0.007	0.37	0.824	0.37	0.825
pH*pH	0.20	0.903	0.1	0.911	0.05	0.823	0.01	0.917	0.01	0.914	0.03	0.870	0.39	0.014	0.56	0.463	0.67	0.004
Conc*Conc	0.16	0.690	0.36	0.559	0.35	0.562	0.11	0.747	0.27	0.608	0.05	0.870	0.45	0.510	0.46	0.506	0.41	0.533
Time*Time	7.01	0.018	5.75	0.029	9.31	0.008	7.78	0.013	10.02	0.006	7.98	0.012	1.35	0.262	0.76	0.398	0.67	0.425
Temp*Temp	0.21	0.657	0.81	0.381	0.00	0.985	0.08	0.783	0.05	0.834	0.20	0.664	0.00	0.019	0.00	0.946	0.00	0.998
2-Way Inter	1.57	0.219	2.48	0.068	2.24	0.092	2.40	0.076	2.69	0.053	2.18	0.100	0.29	0.935	0.30	0.930	0.26	0.948
pH*Conc	0.21	0.654	0.42	0.528	0.41	0.530	0.72	0.409	0.06	0.804	0.30	0.589	1.10	0.010	1.15	0.002	1.07	0.317
pH*Time	3.60	0.076	4.68	0.046	4.34	0.054	4.31	0.054	7.46	0.015	4.70	0.046	0.22	0.016	0.14	0.716	0.12	0.731
pH*Temp	1.11	0.307	2.19	0.158	1.50	0.238	1.93	0.184	1.69	0.213	1.62	0.221	0.23	0.035	0.24	0.629	0.20	0.065
Conc*Time	0.18	0.679	0.12	0.737	0.24	0.633	0.02	0.901	0.11	0.746	0.43	0.522	0.00	0.979	0.00	0.945	0.01	0.040
Conc*Temp	0.60	0.451	0.64	0.437	1.23	0.284	0.92	0.353	1.14	0.302	1.14	0.302	0.07	0.795	0.07	0.795	0.05	0.834
Time*Temp	3.74	0.071	6.86	0.021	5.73	0.029	6.48	0.022	5.68	0.03	4.85	0.043	0.10	0.754	0.16	0.691	0.11	0.743
Lack of Fit	3.48	0.070	6.86	0.019	5.73	0.029	6.48	0.022	5.68	0.030	4.85	0.043	0.88	0.059	1.07	0.049	0.94	0.056
Pure Error	6	6	6	6	6	6	6	6	6	6	6	6	16	16	16	16	16	16

$p < 0.01$ highly significant; $0.01 < p < 0.05$ significant; $p > 0.05$ not significant.

The 3D surfaces and 2D contour plots for a function of two parameters are shown to examine the effects of more than one parameter on the removal percentage of heavy metals (HMs). While keeping other parameters constant, this diagram depicts the relative influence of any two variables. The plots of the three-dimensional response surfaces (3D) and contour curves (2D) depicting the major interactions of the parameters with heavy metals are shown in Figure 12A–Ei. Figure 12A–C show the interaction of pH and concentration for the removal of nickel, cadmium, and lead, respectively, with removal percentages of heavy metals. The surface response shows that the removal percentage of all the heavy metals increased as pH increased with an increase in the concentration of the solution. Similarly, the interaction of pH and time in Figure 12C–E revealed that the removal percentages were higher in the alkaline medium around pH 8–10.

3.3.4. Ball-Milled Biochar Application in a Real Wastewater Sample

Standardised mixed solutions of the steroidal hormones and heavy metals at 2.5 mg L^{-1} were spiked with a 25 mL wastewater sample (effluent and influent). The removal capacity of the adsorbent was investigated using the optimal conditions. Table 7 shows the removal efficiency for the effluent and influent; the highest adsorption percentage was between 84–89% and 78–86%, respectively. The results indicate a considerable decline in the removal efficiency of steroidal hormones and heavy metals in the wastewater sample. In comparison, the increased removal efficiency of the standard mixed solution made with ultrapure water containing known amounts of steroidal hormones and heavy metals was shown to have a removal efficiency of between 91 and 95%. This reduction could be explained by the presence of several competing ions in the wastewater sample, which were presumably vying for the available active sites on the surface of the BMB500.

3.3.5. Reusability of the Ball-Milled Biochar

High adsorption capacity and sustainable usage of an adsorbent are unique characteristics that a promising adsorbent should possess. The reusability of adsorbents is essential for a cost-effective, long-term pollutant removal. Figure 13 depicts the regenerated BMB500 adsorption performance. The adsorption capacity of regenerated biochar declined steadily, as can be seen in Figure 13. When comparing the first and fifth cycles, the adsorption ability of BMB500 only dropped significantly below 60% after the fourth cycle. The decrease in the adsorption capacity of the BMB500 after each desorption experiment can be ascribed to the loss of functional groups on the BMB500's surface [46]. The result of these experimental findings showed that the adsorbent (BMB500) had good regeneration efficiency for the first four cycles and could be successfully re-used four times. As a result, the ball-milled modified biochar might be employed as a sustainable adsorbent for the simultaneous removal of steroidal hormones and heavy metals in water and wastewater.
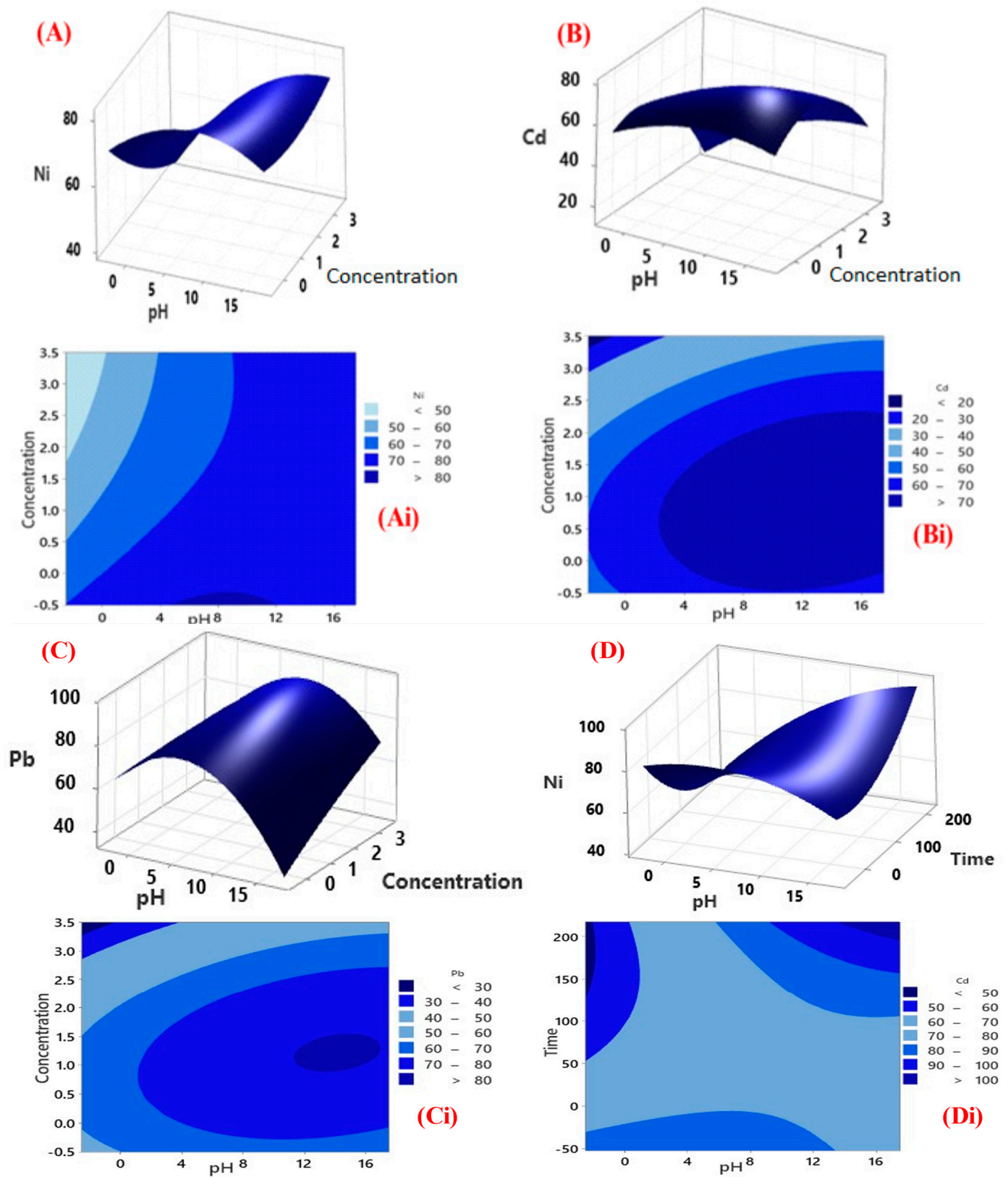
Figure 12. *Cont.*
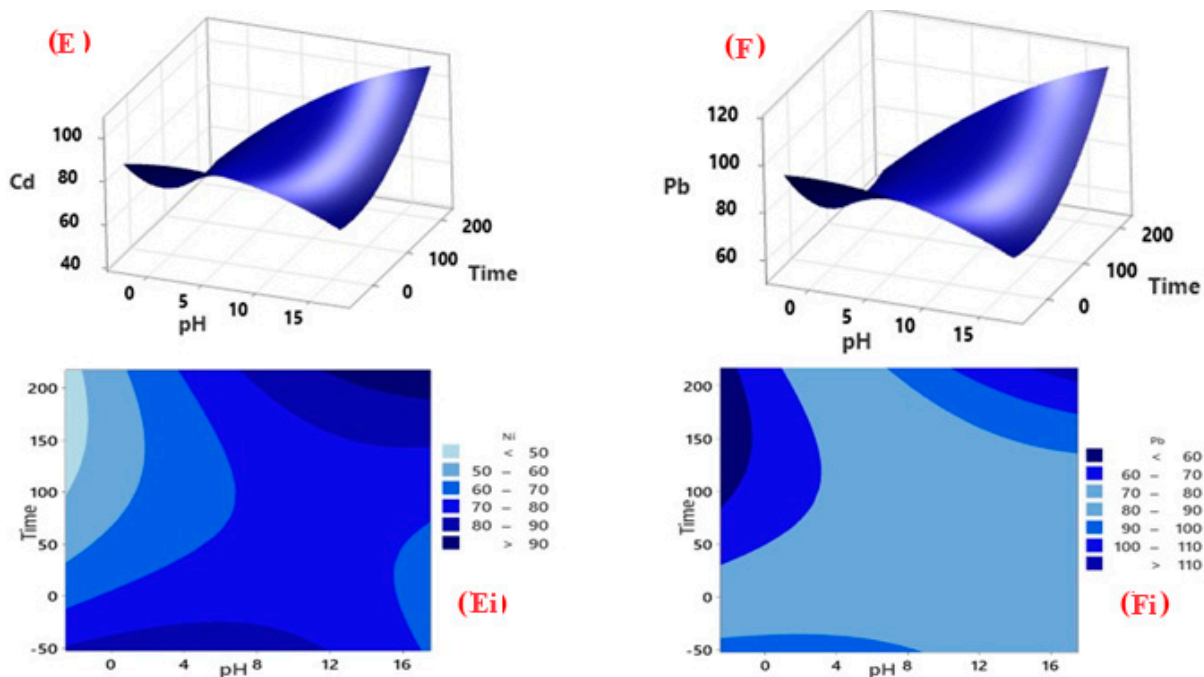
Figure 12. Three-dimensional (3D) SRM and (2D) counterplots for interaction effects of factors for HM removal by BMB500.

Table 7. Ball-milled biochar (BMB500) removal efficiency in UPH water and real wastewater sample.

Analyte	Ultrapure Water (% Removal)	Effluent (% Removal)	Influent (% Removal)
Estriol	93	87	85
α-Oestradiol	90	86	83
β-Oestradiol	91	88	86
Testosterone	92	84	80
Progesterone	95	89	82
Bisphenol A	94	86	78
Nickel	91	83	75
Cadmium	90	87	83
Lead	93	85	84
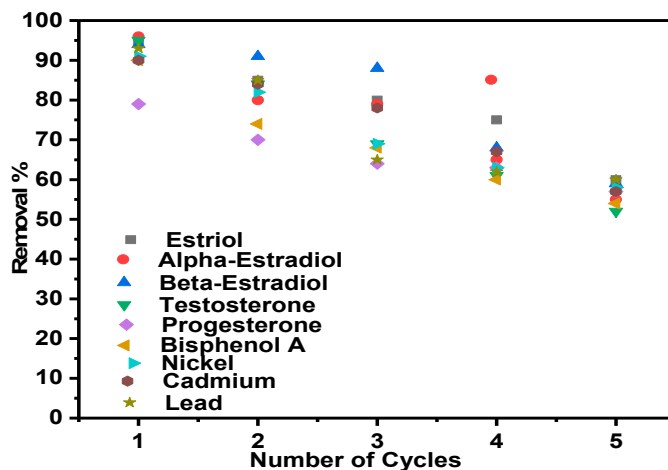
Figure 13. Reusability of BMB500 for the efficient removal of steroidal hormones and heavy metals regenerated by ethanol.

4. Conclusions

This study investigated the adsorption characteristics of BMB500 nano-sized biochar modified by the facile ball-milling method for the synergetic removal of selected groups of steroidal hormones (estriol, β-oestradiol, α-oestradiol, testosterone, progesterone, and bisphenol A) and heavy metals (nickel, cadmium, and lead) simultaneously from wastewater. To understand the physicochemical properties of the ball-milled biochar, the BMB500 was characterised using BET, XRD, FTIR, SEM-EDS, TGA, XPS, and Raman spectroscopy to examine the surface morphology, crystallinity, thermal stability, and functional groups of the nano-sized ball-milled biochar. The BET results indicated a significant increase in the surface area and reduction in the size of the ball-milled biochar. The surface area increased significantly after ball-milling modification from 53.1 m^2/g (B400) to 275.9 m^2/g (BMB500), from 220.1 m^2/g (B500) to 354.6 m^2/g (BMB500), and from 278.6 m^2/g (B600) to 311 m^2/g (BMB600). XPS and FTIR analyses also revealed the presence of functional groups that could be attributed to the binding sites for the steroidal hormones. SEM-EDS showed the morphology and elemental composition of the biochar. XRD also revealed the effect of the fast-moving balls on the pristine biochar, changing the structure from partially crystalline to totally amorphous after ball milling. The TGA showed the excellent thermal properties of ideal carbonaceous materials of the ball-milled biochar, which was thermally stable up to 600 °C. A full factorial 2^5 experimental design using Minitab Statistical software '21' was employed to optimise the adsorption experimental conditions. The following factors and levels were included in the design of the experiments: pH, concentration, time, and temperature. The F-value and the high *p*-values for lack-of-fit of the model for the SHs indicated the acceptability of the ANOVA model and significance in demonstrating the relationship between the component variables and the response process. The adsorption experiment was found to be fitted better to the Freundlich isotherm than the Langmuir model, with moderate values of $R^2 \geq 0.92$ for Langmuir and $R^2 \geq 0.95$ for Freundlich, as well as maximum adsorption capacities of 14.53 (mg g^{-1}), 10.58 (mg g^{-1}), 12.50 (mg g^{-1}), 5.73 (mg g^{-1}), 5.63 (mg g^{-1}), and 9.75 (mg g^{-1}) for estriol, α-oestradiol, β-oestradiol, testosterone, progesterone, and bisphenol, respectively. Similarly, values of $R^2 \geq 0.98$ for Langmuir and $R^2 \geq 0.78$ for Freundlich were obtained for heavy metals, with maximum adsorption capacities of 8.58 (mg g^{-1}), 4.15(mg g^{-1}), and 6.95 (mg g^{-1}) for nickel, cadmium, and lead, respectively. Additionally, the favourable values of K_f >1 from the Freundlich isotherm model suggest that chemosorption adsorption was well favoured during the adsorption of the steroidal hormones and heavy metals. In addition, the favourable values of n between 0 and 1 from the Freundlich isotherm model suggest that multilayer adsorption on the heterogenous surface was well favoured during the adsorption of the steroidal hormones and heavy metals. The application of the ball-milled biochar was put to the test on real wastewater samples obtained from a wastewater treatment plant and the results demonstrated that the adsorbent was effective for removing steroidal hormones and heavy metals from the wastewater sample. The maximum percentage removal values of 84–89%, 78–86%, and 90–95% were obtained for effluent, influent, and spiked ultrapure water, respectively. The reusability of the ball-milled biochar produced was also investigated, and the result of the experimental findings showed that the adsorbent (BMB500) had a high regeneration efficiency for the first four cycles and could be re-used successfully up to four times. As a result, the ball-milled modified biochar might be employed as a sustainable adsorbent for the removal of steroidal hormones and heavy metals from water and wastewater.

References

1. Zhang, Q.-Q.; Xing, C.; Cai, Y.-Y.; Yan, X.-T.; Ying, G.-G. How much do human and livestock actually contribute to steroids emission and surface water pollution from past to the future: A global research. *Sci. Total Environ.* **2021**, *772*, 145558. [CrossRef]
2. Rahman, M.M.; Rana, R.; Khanam, R. Determinants of life expectancy in most polluted countries: Exploring the effect of environmental degradation. *PLoS ONE* **2022**, *17*, e0262802. [CrossRef]
3. Chakraborty, P.; Shappell, N.W.; Mukhopadhyay, M.; Onanong, S.; Rex, K.R.; Snow, D. Surveillance of plasticizers, bisphenol A, steroids and caffeine in surface water of River Ganga and Sundarban wetland along the Bay of Bengal: Occurrence, sources, estrogenicity screening and ecotoxicological risk assessment. *Water Res.* **2021**, *19*, 116668. [CrossRef]
4. Azizi-lalabadi, M.; Pirsaheb, M. Investigation of Steroid Hormone Residues in Fish: A Systematic Review. *Process Saf. Environ. Prot.* **2021**, *152*, 14–24. [CrossRef]
5. Zhong, R.; Zou, H.; Gao, J.; Wang, T.; Bu, Q.; Wang, Z.L.; Hu, M.; Wang, Z. A critical review on the distribution and ecological risk assessment of steroid hormones in the environment in China. *Sci. Total Environ.* **2021**, *786*, 147452. [CrossRef]
6. Zheng, X.; Zhang, K.; Zhao, Y.; Fent, K. Environmental chemicals affect circadian rhythms: An underexplored effect influencing health and fitness in animals and humans. *Environ. Int.* **2021**, *149*, 106159. [CrossRef]
7. Parrott, J.L.; Blunt, B.R. Life-cycle exposure of fathead minnows (*Pimephales promelas*) to an ethinylestradiol concentration below 1 ng/L reduces egg fertilization success and demasculinizes males. *Environ. Toxicol.* **2005**, *20*, 131–141. [CrossRef]
8. Chang, M. Dual roles of estrogen metabolism in mammary carcinogenesis. *BMB Rep.* **2011**, *44*, 423–434. [CrossRef]
9. Vasto, S.; Carruba, G.; Candore, G.; Italiano, E.; Di Bona, D.; Caruso, C. Inflammation and prostate cancer. *Futur. Oncol.* **2008**, *4*, 637–645. [CrossRef]
10. Brachet, C.; Heinrichs, C. Central precocious puberty after interpersonal transfer of testosterone gel: Just a coincidence? *J. Pediatr. Endocrinol. Metab.* **2012**, *25*, 757–760. [CrossRef]
11. Lyssimachou, A.; Arukwe, A. Alteration of brain and interrenal StAR protein, P450 scc, and Cyp11β mRNA levels in Atlantic Salmon after nominal waterborne exposure to the synthetic pharmaceutical estrogen ethynylestradiol. *J. Toxicol. Environ. Heal. Part. A* **2007**, *70*, 606–613. [CrossRef]
12. Neczaj, E. Fate of selected emerging contaminants in wastewater treatment systems. *Desalin. Water Treat.* **2020**, *199*, 451–463. [CrossRef]
13. Archer, E.; Petrie, B.; Kasprzyk-Hordern, B.; Wolfaardt, G.M. The fate of pharmaceuticals and personal care products (PPCPs), endocrine disrupting contaminants (EDCs), metabolites and illicit drugs in a WWTW and environmental waters. *Chemosphere* **2017**, *174*, 437–446. [CrossRef] [PubMed]
14. Mhuka, V.; Dube, S.; Nindi, M.M. Occurrence of pharmaceutical and personal care products (PPCPs) in wastewater and receiving waters in South Africa using LC-Orbitrap^{TM} MS. *Emerg. Contam.* **2020**, *6*, 250–258. [CrossRef]
15. Naddafi, K.; Mesdaghinia, A.; Abtahi, M.; Hassanvand, M.S.; Beiki, A.; Shaghaghi, G.; Shamsipour, M.; Mohammadi, F.; Saeedi, R. Assessment of burden of disease induced by exposure to heavy metals through drinking water at national and subnational levels in Iran, 2019. *Environ. Res.* **2022**, *204*, 112057. [CrossRef]
16. Gade, M.; Comfort, N.; Re, D.B. Sex-specific neurotoxic effects of heavy metal pollutants: Epidemiological, experimental evidence and candidate mechanisms. *Environ. Res.* **2021**, *201*, 111558. [CrossRef]
17. Sun, D.T.; Peng, L.; Reeder, W.S.; Moosavi, S.M.; Tiana, D.; Britt, D.K.; Oveisi, E.; Queen, W.L. Rapid, selective heavy metal removal from water by a metal–organic framework/polydopamine composite. *ACS Cent. Sci.* **2018**, *4*, 349–356. [CrossRef] [PubMed]
18. Majdoub, M.; Amedlous, A.; Anfar, Z.; Jada, A.; El Alem, N. Engineering of amine-based binding chemistry on functionalized graphene oxide/alginate hybrids for simultaneous and efficient removal of trace heavy metals: Towards drinking water. *J. Colloid. Interface Sci.* **2021**, *589*, 511–524. [CrossRef]
19. Nys, C.; Versieren, L.; Cordery, K.I.; Blust, R.; Smolders, E.; De Schamphelaere, K.A.C. Systematic evaluation of chronic metal-mixture toxicity to three species and implications for risk assessment. *Environ. Sci. Technol.* **2017**, *51*, 4615–4623. [CrossRef]

20. Noutsopoulos, C.; Katsigiannis, A.; Mantziaras, J.; Gioldasi, M.; Katsiri, A. Removal of Anti-Inflammatory Drugs and Endocrine Disrupting Compounds By Granular Activated Carbon. In Proceedings of the International Conference on Environmental Science and Technology, Athens, Greece, 5–7 September 2013.

21. Peydayesh, M.; Bolisetty, S.; Mohammadi, T.; Mezzenga, R. Assessing the Binding Performance of Amyloid-Carbon Membranes toward Heavy Metal Ions. *Langmuir* **2019**, *35*, 4161–4170. [CrossRef]

22. Lyu, H.; Xia, S.; Tang, J.; Zhang, Y.; Gao, B.; Shen, B. Thiol-modified biochar synthesized by a facile ball-milling method for enhanced sorption of inorganic Hg^{2+} and organic CH_3Hg^+. *J. Hazard. Mater.* **2020**, *384*, 121357. [CrossRef] [PubMed]

23. Jean, E.; Villemin, D.; Hlaibi, M.; Lebrun, L. Heavy metal ions extraction using new supported liquid membranes containing ionic liquid as carrier. *Sep. Purif. Technol.* **2018**, *201*, 1–9. [CrossRef]

24. Nekouei, R.K.; Pahlevani, F.; Assefi, M.; Maroufi, S.; Sahajwalla, V. Selective isolation of heavy metals from spent electronic waste solution by macroporous ion-exchange resins. *J. Hazard. Mater.* **2019**, *371*, 389–396. [CrossRef] [PubMed]

25. Shariful, M.I.; Sepehr, T.; Mehrali, M.; Ang, B.C.; Amalina, M.A. Adsorption capability of heavy metals by chitosan/poly (ethylene oxide)/activated carbon electrospun nanofibrous membrane. *J. Appl. Polym. Sci.* **2018**, *135*, 45851. [CrossRef]

26. Vieira, W.T.; de Farias, M.B.; Spaolonzi, M.P.; da Silva, M.G.C.; Vieira, M.G.A. Removal of endocrine disruptors in waters by adsorption, membrane filtration and biodegradation. A review. *Environ. Chem. Lett.* **2020**, *18*, 1113–1143. [CrossRef]

27. Vital, B.; Bartacek, J.; Ortega-Bravo, J.C.; Jeison, D. Treatment of acid mine drainage by forward osmosis: Heavy metal rejection and reverse flux of draw solution constituents. *Chem. Eng. J.* **2018**, *332*, 85–91. [CrossRef]

28. Li, Y.-H.; Ding, J.; Luan, Z.; Di, Z.; Zhu, Y.; Xu, C.; Wu, D.; Wei, B. Competitive adsorption of Pb^{2+}, Cu^{2+} and Cd^{2+} ions from aqueous solutions by multiwalled carbon nanotubes. *Carbon* **2003**, *41*, 2787–2792. [CrossRef]

29. Wang, X.; Liu, N.; Liu, Y.; Jiang, L.; Zeng, G.; Tan, X.; Liu, S.; Yin, Z.; Tian, S.; Li, J. Adsorption removal of 17β-estradiol from water by rice straw-derived biochar with special attention to pyrolysis temperature and background chemistry. *Int. J. Environ. Res. Public Health* **2017**, *14*, 1213. [CrossRef]

30. Zaib, Q.; Khan, I.A.; Saleh, N.B.; Flora, J.R.V.; Park, Y.G.; Yoon, Y. Removal of bisphenol a and 17β-estradiol by single-walled carbon nanotubes in aqueous solution: Adsorption and molecular modeling. *Water. Air. Soil Pollut.* **2012**, *223*, 3281–3293. [CrossRef]

31. Wan, S.; Wang, S.; Li, Y.; Gao, B. Functionalizing biochar with Mg–Al and Mg–Fe layered double hydroxides for removal of phosphate from aqueous solutions. *J. Ind. Eng. Chem.* **2017**, *47*, 246–253. [CrossRef]

32. Das, P.; Nisa, S.; Debnath, A.; Saha, B. Enhanced adsorptive removal of toxic anionic dye by novel magnetic polymeric nanocomposite: Optimization of process parameters. *J. Dispers. Sci. Technol.* **2022**, *43*, 880–895. [CrossRef]

33. Deb, A.; Debnath, A.; Bhowmik, K.; Paul, S.R.; Saha, B. Application of polyaniline impregnated mixed phase Fe_2O_3, $MnFe_2O_4$ and ZrO_2 nanocomposite for rapid abatement of binary dyes from aqua matrix: Response surface optimisation. *Int. J. Environ. Anal. Chem.* **2021**, 1–19. [CrossRef]

34. Das, P.; Debnath, A. Reactive orange 12 dye adsorption onto magnetically separable CaFe2O4 nanoparticles synthesized by simple chemical route: Kinetic, isotherm and neural network modeling. *Water Pract. Technol.* **2021**, *16*, 1141–1158. [CrossRef]

35. Cheng, N.; Wang, B.; Wu, P.; Lee, X.; Xing, Y.; Chen, M.; Gao, B. Adsorption of emerging contaminants from water and wastewater by modified biochar: A review. *Environ. Pollut.* **2021**, *273*, 116448. [CrossRef]

36. Inyang, M.; Dickenson, E. The potential role of biochar in the removal of organic and microbial contaminants from potable and reuse water: A review. *Chemosphere* **2015**, *134*, 232–240. [CrossRef]

37. Peiris, C.; Nawalage, S.; Wewalwela, J.J.; Gunatilake, S.R.; Vithanage, M. Biochar based sorptive remediation of steroidal estrogen contaminated aqueous systems: A critical review. *Environ. Res.* **2020**, *191*, 110183. [CrossRef]

38. Huang, J.; Zimmerman, A.R.; Chen, H.; Gao, B. Ball milled biochar effectively removes sulfamethoxazole and sulfapyridine antibiotics from water and wastewater. *Environ. Pollut.* **2020**, *258*, 113809. [CrossRef]

39. Jang, H.M.; Kan, E. Engineered biochar from agricultural waste for removal of tetracycline in water. *Bioresour. Technol.* **2019**, *284*, 437–447. [CrossRef]

40. Gholami, P.; Dinpazhoh, L.; Khataee, A.; Hassani, A.; Bhatnagar, A. Facile hydrothermal synthesis of novel Fe-Cu layered double hydroxide/biochar nanocomposite with enhanced sonocatalytic activity for degradation of cefazolin sodium. *J. Hazard. Mater.* **2020**, *381*, 120742. [CrossRef]

41. Amusat, S.O.; Kebede, T.G.; Dube, S.; Nindi, M.M. Ball-milling synthesis of biochar and biochar–based nanocomposites and prospects for removal of emerging contaminants: A review. *J. Water Process Eng.* **2021**, *41*, 101993. [CrossRef]

42. Karvelas, M.; Katsoyiannis, A.; Samara, C. Occurrence and fate of heavy metals in the wastewater treatment process. *Chemosphere* **2003**, *53*, 1201–1210. [CrossRef] [PubMed]

43. Lyu, H.; Gao, B.; He, F.; Zimmerman, A.R.; Ding, C.; Tang, J.; Crittenden, J.C. Experimental and modeling investigations of ball-milled biochar for the removal of aqueous methylene blue. *Chem. Eng. J.* **2018**, *355*, 110–119. [CrossRef]

44. Shan, D.; Deng, S.; Zhao, T.; Wang, B.; Wang, Y.; Huang, J.; Yu, G.; Winglee, J.; Wiesner, M.R. Preparation of ultrafine magnetic biochar and activated carbon for pharmaceutical adsorption and subsequent degradation by ball milling. *J. Hazard. Mater.* **2016**, *305*, 156–163. [CrossRef] [PubMed]

45. Kebede, T.G.; Dube, S.; Nindi, M.M. Characterisation of water-soluble protein powder and optimisation of process parameters for the removal of sulphonamides from wastewater. *Environ. Sci. Pollut. Res.* **2019**, *26*, 21450–21462. [CrossRef]

46. Mekala, M.; Neerudi, B.; Are, P.R.; Surakasi, R.; Manikandan, G.; Kakara, V.R.; Dhumal, A.A. Water removal from an ethanol-water mixture at azeotropic condition by adsorption technique. *Adsorpt. Sci. Technol.* **2022**, *2022*, 10. [CrossRef]

47. Zhang, D.; He, Q.; Hu, X.; Zhang, K.; Chen, C.; Xue, Y. Enhanced adsorption for the removal of tetracycline hydrochloride (TC) using ball-milled biochar derived from crayfish shell. *Colloids Surfaces A Physicochem. Eng. Asp.* **2021**, *615*, 126254. [CrossRef]

48. Elnour, A.Y.; Alghyamah, A.A.; Shaikh, H.M.; Poulose, A.M.; Al-Zahrani, S.M.; Anis, A.; Al-Wabel, M.I. Effect of pyrolysis temperature on biochar microstructural evolution, physicochemical characteristics, and its influence on biochar/polypropylene composites. *Appl. Sci.* **2019**, *9*, 1149. [CrossRef]

49. Zhang, Q.; Wang, J.; Lyu, H.; Zhao, Q.; Jiang, L.; Liu, L. Ball-milled biochar for galaxolide removal: Sorption performance and governing mechanisms. *Sci. Total Environ.* **2019**, *659*, 1537–1545. [CrossRef]

50. Kumar, N.S.; Shaikh, H.M.; Asif, M.; Al-Ghurabi, E.H. Engineered biochar from wood apple shell waste for high-efficient removal of toxic phenolic compounds in wastewater. *Sci. Rep.* **2021**, *11*, 2586. [CrossRef]

51. Fang, Z.; Gao, Y.; Bolan, N.; Shaheen, S.M.; Xu, S.; Wu, X.; Xu, X.; Hu, H.; Lin, J.; Zhang, F. Conversion of biological solid waste to graphene-containing biochar for water remediation: A critical review. *Chem. Eng. J.* **2020**, *390*, 124611. [CrossRef]

52. Gupta, N.K.; Prakash, P.; Kalaichelvi, P.; Sheeba, K.N. The effect of temperature and hemicellulose-lignin, cellulose-lignin, and cellulose-hemicellulose on char yield from the slow pyrolysis of rice husk. Energy Sources Part A Recover. *Util. Environ. Eff.* **2016**, *38*, 1428–1434.

53. Sarmah, A.K.; Srinivasan, P.; Smernik, R.J.; Manley-Harris, M.; Antal, M.J.; Downie, A.; Van Zwieten, L. Retention capacity of biochar-amended New Zealand dairy farm soil for an estrogenic steroid hormone and its primary metabolite. *Aust. J. Soil. Res.* **2010**, *48*, 648–658. [CrossRef]

54. Wang, W.; Gong, Q.; Chen, Z.; Wang, W.D.; Huang, Q.; Song, S.; Chen, J.; Wang, X. Adsorption and competition investigation of phenolic compounds on the solid-liquid interface of three-dimensional foam-like graphene oxide. *Chem. Eng. J.* **2019**, *378*, 122085. [CrossRef]

55. Smidt, E.; Meissl, K. The applicability of Fourier transform infrared (FT-IR) spectroscopy in waste management. *Waste Manag.* **2007**, *27*, 268–276. [CrossRef] [PubMed]

56. Schwanninger, M.; Rodrigues, J.C.; Pereira, H.; Hinterstoisser, B. Effects of short-time vibratory ball milling on the shape of FT-IR spectra of wood and cellulose. *Vib. Spectrosc.* **2004**, *36*, 23–40. [CrossRef]

57. Tatzber, M.; Stemmer, M.; Spiegel, H.; Katzlberger, C.; Haberhauer, G.; Mentler, A.; Gerzabek, M.H. FTIR-spectroscopic characterization of humic acids and humin fractions obtained by advanced NaOH, $Na_4P_2O_7$, and Na $2CO_3$ extraction procedures. *J. Plant Nutr. Soil Sci.* **2007**, *170*, 522–529. [CrossRef]

58. Xu, X.; Xu, Z.; Huang, J.; Gao, B.; Zhao, L.; Qiu, H.; Cao, X. Sorption of reactive red by biochars ball milled in different atmospheres: Co-effect of surface morphology and functional groups. *Chem. Eng. J.* **2021**, *413*, 127468. [CrossRef]

59. Zhao, S.X.; Ta, N.; Wang, X.D. Effect of temperature on the structural and physicochemical properties of biochar with apple tree branches as feedstock material. *Energies* **2017**, *10*, 1293. [CrossRef]

60. Naderi, H.R.; Norouzi, P.; Ganjali, M.R. Electrochemical study of a novel high performance supercapacitor based on MnO_2/nitrogen-doped graphene nanocomposite. *Appl. Surf. Sci.* **2016**, *366*, 552–560. [CrossRef]

61. Bajpai, V.K.; Shukla, S.; Khan, I.; Kang, S.-M.; Haldorai, Y.; Tripathi, K.M.; Jung, S.; Chen, L.; Kim, T.; Huh, Y.S. A sustainable graphene aerogel capable of the adsorptive elimination of biogenic amines and bacteria from soy sauce and highly efficient cell proliferation. *ACS Appl. Mater. Interfaces* **2019**, *11*, 43949–43963. [CrossRef]

62. Xiang, W.; Wan, Y.; Zhang, X.; Tan, Z.; Xia, T.; Zheng, Y.; Gao, B. Adsorption of tetracycline hydrochloride onto ball-milled biochar: Governing factors and mechanisms. *Chemosphere* **2020**, *255*, 127057. [CrossRef] [PubMed]

63. Wang, H.; Liu, Y.; Li, M.; Huang, H.; Xu, H.; Hong, R.; Shen, H. Multifunctional TiO2 nanowires-modified nanoparticles bilayer film for 3D dye-sensitized solar cells. *Optoelectron. Adv. Mater. Commun.* **2010**, *4*, 1166–1169.

64. Fan, Z.; Zhang, Q.; Gao, B.; Li, M.; Liu, C.; Qiu, Y. Removal of hexavalent chromium by biochar supported nZVI composite: Batch and fixed-bed column evaluations, mechanisms, and secondary contamination prevention. *Chemosphere* **2019**, *217*, 85–94. [CrossRef] [PubMed]

65. Bokova, S.N.; Obraztsova, E.D.; Grebenyukov, V.V.; Elumeeva, K.V.; Ishchenko, A.V.; Kuznetsov, V.L. Raman diagnostics of multi-wall carbon nanotubes with a small wall number. *Phys. Status Solidi Basic Res.* **2010**, *247*, 2827–2830. [CrossRef]

66. Xing, T.; Li, L.H.; Hou, L.; Hu, X.; Zhou, S.; Peter, R.; Petravic, M.; Chen, Y. Disorder in ball-milled graphite revealed by Raman spectroscopy. *Carbon* **2013**, *57*, 515–519. [CrossRef]

67. El-Khaiary, M.I. Least-squares regression of adsorption equilibrium data: Comparing the options. *J. Hazard. Mater.* **2008**, *158*, 73–87. [CrossRef]

68. Dąbrowski, A. Adsorption—From theory to practice. *Adv. Colloid Interface Sci.* **2001**, *93*, 135–224. [CrossRef]

69. Ayawei, N.; Angaye, S.S.; Wankasi, D.; Dikio, E.D. Synthesis, Characterization and Application of Mg/Al Layered Double Hydroxide for the Degradation of Congo Red in Aqueous Solution. *Open J. Phys. Chem.* **2015**, *5*, 56–70. [CrossRef]

70. Ayawei, N.; Ekubo, A.T.; Wankasi, D.; Dikio, E.D. Adsorption of congo red by Ni/Al-CO3: Equilibrium, thermodynamic and kinetic studies. *Orient. J. Chem.* **2015**, *31*, 1307. [CrossRef]

71. Khuri, A.I.; Mukhopadhyay, S. Response surface methodology. *Wiley Interdiscip. Rev. Comput. Stat.* **2010**, *2*, 128–149. [CrossRef]

72. Tong, S.; Chen, N.; Wang, H.; Liu, H.; Tao, C.; Feng, C.; Zhang, B.; Hao, C.; Pu, J.; Zhao, J. Optimization of C/N and current density in a heterotrophic/biofilm-electrode autotrophic denitrification reactor (HAD-BER). *Bioresour. Technol.* **2014**, *171*, 389–395. [CrossRef] [PubMed]

73. Asadzadeh, F.; Maleki-Kaklar, M.; Soiltanalinejad, N.; Shabani, F. Central composite design optimization of zinc removal from contaminated soil, using citric acid as biodegradable chelant. *Sci. Rep.* **2018**, *8*, 1–8. [CrossRef]

74. Lima, E.C.; Royer, B.; Vaghetti, J.C.P.; Brasil, J.L.; Simon, N.M.; dos Santos, A.A., Jr.; Pavan, F.A.; Dias, S.L.P.; Benvenutti, E.V.; da Silva, E.A. Adsorption of Cu (II) on Araucaria angustifolia wastes: Determination of the optimal conditions by statistic design of experiments. *J. Hazard. Mater.* **2007**, *140*, 211–220. [CrossRef] [PubMed]

75. Safa, Y.; Bhatti, H.N.; Bhatti, I.A.; Asgher, M. Removal of direct Red-31 and direct Orange-26 by low cost rice husk: Influence of immobilisation and pretreatments. *Can. J. Chem. Eng.* **2011**, *89*, 1554–1565. [CrossRef]

76. El-Sesy, M.E.; Ibrahim, S.S. Application of central composite design approach for optimization nitrate removal from aqueous solution by immobilized Pseudomonas putida. *Water Sci. Technol.* **2021**, *83*, 2931–2946. [CrossRef]

77. Carley, K.M.; Kamneva, N.Y.; Reminga, J. *Response Surface Methodology*; Carnegie-Mellon University: Pittsburgh, PA, USA, 2004.

78. Moradi, M.; Fazlzadehdavil, M.; Pirsaheb, M.; Mansouri, Y.; Khosravi, T.; Sharafi, K. Response surface methodology (RSM) and its application for optimization of ammonium ions removal from aqueous solutions by pumice as a natural and low cost adsorbent. *Arch. Environ. Prot.* **2016**, *42*, 33–43. [CrossRef]

79. Wu, J.; Zhang, H.; Oturan, N.; Wang, Y.; Chen, L.; Oturan, M.A. Application of response surface methodology to the removal of the antibiotic tetracycline by electrochemical process using carbon-felt cathode and DSA (Ti/RuO$_2$–IrO$_2$) anode. *Chemosphere* **2012**, *87*, 614–620. [CrossRef]

80. Jafari, A.; Mahvi, A.H.; Godini, H.; Rezaee, R.; Hosseini, S.S. Process optimization for fluoride removal from water by Moringa oleifera seed extract. *Fluoride* **2014**, *47*, 152–160.